NOVA SCHOOL OF SCIENCE & TECHNOLOGY

DEPARTAMENT OF MATERIALS

Daniel Filipe Correia Marques Rodrigues

BSc in Micro and Nanotechnology Engineering

Plasmonic-driven thermal sensing: Ultralow detection of Influenza Virus

MASTER IN MICRO AND NANOTECHNOLOGY ENGINEERING

NOVA University Lisbon

September, 2023

NOVA SCHOOL OF SCIENCE & TECHNOLOGY

DEPARTAMENT OF MATERIALS

Plasmonic-driven thermal sensing: Ultralow detection of Influenza Virus

Daniel Filipe Correia Marques Rodrigues

BSc in Micro and Nanotechnology Engineering

Adviser: Carlos Cuesta Ayllón
Full Professor, Zaragoza University

Co-advisers: José Ricardo Ramos Franco Tavares
Full Professor, NOVA FCT Lisbon University

Examination Committee:

Chair: Hugo Manuel Brito Águas,
Associate Professor, NOVA FCT Lisbon University

Rapporteurs: Catarina Roma Rodrigues,
Associate Professor, Another University

Adviser: Carlos Cuestas Ayllón,
Full Professor, Zaragoza University

MASTER IN MICRO AND NANOTECHNOLOGY ENGINEERING

NOVA University Lisbon
September,2023

Plasmonic-driven thermal sensing: Ultralow detection of Influenza Virus

ACKNOWLEDGMENTS

To start, I would like to thank my advisors, Researcher Carlos Cuestas and Professor Ricardo Franco. To Professor Ricardo Franco, I would like to thank you for all your support, guidance, and willingness to help, for all the knowledge you've passed on during these months, and for recommending this thesis proposal that took me completely out of my comfort zone. It was a challenge, but I'm sure I managed to overcome it and bring with me new skills and qualities for my future. I would like to thank Researcher Carlos Cuestas for welcoming me so well into his working group, putting up with all my doubts about pure chemistry and for helping me whenever I needed help. I would also like to thank Professor Jesús de la Fuente for accepting me and integrating me into this project, which has led me to overcome challenges I hadn't imagined.

I would like to thank both the University of Aveiro and my University, FCT NOVA, which have been my second home throughout these five years. I would also like to thank the University of Zaragoza (UNIZAR), especially the BioNanoSurf group, for giving me the opportunity to develop my thesis, allowing me to grow and learn about nanotechnology applications in the field of health.

To my family, Rui Rodrigues (father), Ana Rodrigues (mother), and Miguel Rodrigues (brother), I know I don't say it often, but they are my pride and my greatest support. I want to thank you from the depth of my heart for all the effort you've made with me, not just during this time, but throughout my entire life. I am who I am and I am where I am thanks to you. Thank you so much for everything.

To my BioNanoSurf mates, Carlos Cuestas (El boss), Natalia Tomás (La Profesora), Adrián Pardos (maestro de geles), Marta Rubio (La Professora 2.0), Antonio Luna, Marina G. Bejarano and Maura Rábade, I'd like to thank you for welcoming me so well into this family, and for all the help and chemistry explanations you've given. And also, for all the good times, laughs and games played during all these months. Todos nosotros nos quedamos esperando por tu mirada sexy del tigre, Adrián.

To my Erasmus friends, Rebecca Nenna, Ieva Nekrošiūtė, Marko Odorjan, Ivana, and others, for all the moments, laughs and memories together. I, also want to thank to my flatmates, Victoria Martinez (enfermera/profesora) for teaching my spanish and that always help me when I was sick, Slávomira Šterbinská (MasterChef) for making that delicious deserts, Esperanza Barranco (mi cariño) for novels and funny moments together, but also thank to all of you for the unforgettable memories and moments. You are always welcome to Portugal.

These 5 years and 2 different faculties have allowed me to meet so many incredible people that I'll always carry them with me and I'm proud to call them friends. To Mariana Duarte, Bárbara Sieira, Manuel Macedo, Mariana Baptista, Bárbara do Carmo, Beatriz Pereira, André Pequito, Ricardo Cabral, Guilherme Correia, Matilde Abreu, Cristiano Barardo, Afonso Azevedo Catarina Lourenço, Lara Pacheco and Rita Pereira, thank you for all your support, laughs, unforgettable memories, and late-night study sessions in the department 7.

“Hard times create strong men. Strong men create good times. Good times create weak men. And, weak men create hard times.” (G. Michael Hopf).

For sure I am not weak…

And for sure these are not weak times…

So, I will not give up because…

“Failure is success in progress.” (Albert Einstein).

ABSTRACT

Laboratory Diagnosis plays an important role in many diseases' management. Early diagnostic is the key to successful treatment providing care at the initial stages. It is especially important in diseases such as viral or bacterial infections and cancer, where time is a crucial factor. Reverse-transcripts real-time polymerase chain reaction (RT-PCR) is the gold standard technique for genetic material detection; however, this method takes several hours. On the other hand, Rapid Diagnostics Tests (RDTs) have been developed to provide quicker results but generally they suffer from lack of sensitivity. Point-of-care (POC) biosensors such as chip-based and paper-based biosensors are typical rapid, cost-effective, and user-friendly RDT, which can be used for genetic material detection. The combination of conventional POC biosensor, how is the lateral flow methodology, with nanomaterials aims to address the previously mentioned problems presented by RDTs. In our peculiar scenario, lateral flow systems have been combined with inorganic nanoparticles, as gold nanoprims (AuNPrs), to develop a novel ultrasensitive Calorimetric Lateral Flow Assay (C-LFA) for Flu A's genetic material detection. Gold nanoprisms (AuNPrs) were biofunctionalized with different synthethic DNA oligonucleotides, complementary to some specific regions within the influenza virus genetic material, working with four different concentrations: [1/1] =$1.36 \times 10^{-3}\ mM$; [1/4] =$3.4 \times 10^{-4}\ mM$; [1/8] =$1.7 \times 10^{-4}\ mM$; [1/16] =$8.5 \times 10^{-5}\ mM$. Due to their optical properties, AuNPrs can convert light into heat. The desired genetic material, RNA in this case, is further recognized by the AuNPrs and the capture biomolecule deposited on the nitrocellulose strip, the subsequent no visible test line irradiation with a NIR laser generates a visible spot in a thermosensitive paper than could can be further quantified. The test on spiked samples demonstrated that the AuNPrs biofunctionalized with oligonucleotides complementary to PB1 viral RNA segment for a concentration of [1/16], presenting a sensitivity in femtomole (fmol) range in complex matrixes as DeltaLab and Biocomma, respectively.

Keywords: Lateral flow assay (LFA), gold nanoprisms (AuNPrs), NIR, Sensitivity, Calorimetric lateral flow assay (C-LFA).

RESUMO

O diagnóstico laboratorial desempenha um papel importante na gestão de muitas doenças. O diagnóstico precoce é a chave para um tratamento bem-sucedido, proporcionando cuidados nas fases iniciais. É especialmente importante em doenças como as infeções virais ou bacterianas e o cancro, em que o tempo é um fator crucial. A transcrição inversa da reação em cadeia da polimerase em tempo real (RT-PCR) é a técnica de referência para a deteção de material genético; no entanto, este método demora várias horas. Por outro lado, os testes de diagnóstico rápido (RDT) foram desenvolvidos para fornecer resultados mais rápidos, mas geralmente sofrem de falta de sensibilidade. Os biossensores de Point-of-Care (POC), tais como os biossensores baseados em *chips* e suporte de papel, são típicos RDTs, económicos e de fácil utilização, que podem ser utilizados para a deteção de material genético. A combinação de um biossensor POC convencional, como um sistema de fluxo lateral, com nanomateriais tem como objetivo resolver os problemas anteriormente mencionados apresentados pelos RDT. No nosso cenário peculiar, os sistemas de fluxo lateral foram combinados com nanopartículas inorgânicas, como os nanoprismas de ouro (AuNPrs), para desenvolver um novo ensaio de fluxo lateral calorimétrico (C-LFA) ultrassensível para a deteção do material genético do Flu A. Os AuNPrs foram biofuncionalizados com diferentes oligonucleótidos de ADN sintéticos, complementares a algumas regiões específicas do material genético do vírus da gripe, trabalhando com quatro diferentes concentrações: [1/1] =$1.36 \times 10^{-3}\ mM$; [1/4] =$3.4 \times 10^{-4}\ mM$; [1/8] =$1.7 \times 10^{-4}\ mM$; [1/16] =$8.5 \times 10^{-5}\ mM$; para reconhecer o material genético desejado e para serem utilizados como transdutores térmicos para o biossensor. Devido às suas propriedades óticas, as AuNPrs podem converter a luz em calor. O material genético desejado, neste caso RNA, é reconhecido pelas AuNPrs e a biomolécula capturada é depositada na tira de nitrocelulose. A subsequente irradiação sem linha de teste visível com um laser NIR gera um ponto visível num papel termossensível que poderá ainda ser quantificado. O teste em amostras contaminadas demonstrou que as AuNPrs biofuncionalizadas com oligonucleótidos complementares ao segmento de RNA viral PB1 para uma concentração de [1/16], apresentam uma sensibilidade na gama de femtmol (fmol) em matrizes complexas como DeltaLab e Biocomma, respetivamente.

Palavras chave: Ensaio de Fluxo Lateral (LFA), nanoprismas de ouro (AuNPrs), NIR, Sensibilidade, Ensaio de Fluxo Lateral Calorimétrico (C-LFA), Z_2T.

CONTENTS

LIST OF FIGURES

LIST OF TABLES

GLOSSARY

Ghost Effect	When the NPrs bypass the test line leaving an empty white square
Flag Effect	When the NPrs do not bypass the test line but leave an intense white square on the test line
Matrix Effect	When we change the matrix of something it can get better or worse

ACRONYMS

LFA	Lateral Flow Assay
CDC	Centres of Disease Control and Prevention
POC	Point-of-Care
C-LFA	Calorimetric Lateral Flow Assay
RDT	Rapid Diagnostic Test
LSPR	Localized Surface Plasmon Resonance
LFIA	Lateral Flow Immuno Assay
CTAB	Cetyltrimethylammonium bromide
TLFA	Thermal Lateral Flow Assay
NPs	Nanoparticles
AuNPs	Gold Nanoparticles
AuNPrs	Gold Nanoprisms
NPrs@oligo	Nanoprisms Biofunctionalized with oligonucleotide
AuNPrs@oligo	Gold Nanoprisms Biofunctionalized with oligonucleotide
AuNPrs@PEG	Gold Nanoprisms synthetized with PEG
AuNPrs@Glutathione	Gold Nanoprisms synthetized with Glutathione
PEG	Polyethylene glycol
PEG-5000D	Polyethylene glycol (HS-C2H4-CONH-PEG-O-C3H6-COOH); MW: 5000 g/mol;
PEG- 750D	Polyethylene glycol (NH2-PEG-OCH3); MW: 750 g/mol;
TBE	Tris-Boric-EDTA
EDTA	Ethylenediaminetetraacetic acid
MQ Water	Deionised water
$\lambda_{Máx}$	Wavelength of maximum absorption
Abs 1050	Absorbance at 1050 nm
Abs 535	Absorbance at 535 nm
MES	2-morpholinoethanesulfonic acid monohydrate
EDC	1-(3-dimethylaminopropyl)-3-ethylcrbodiimidehydrochloride, 98%

Sulfo-NHS	N-hidroxysuccinimide sodium salt
Hepes (99,5%)	N-(2-Hydroxyethyl)piperazine-N´-(2-ehtanesulfonic acid)
BSA	Bovine Serum Albumin
T_{20}	Polyoxyethylene(20)sorbitan Monolaurate (Tween® 20)
Tris	Tris(hydroxymethyl)aminimethane 99%
Sonda	Biotinylated solution of complementary analyte's DNA
RB	Running Buffer
rpm	Rotations per minute
pmol	picomolar (10^{-12})
nm	Nanometers (10^{-9})
LOD	Limit of Detection
MW	Molar Weight
DPS	Sodium Phosphate Dibasic
MSP	Sodium Phosphate Monobasic
PVP-40	Polyvinylpyrrolidone-40
PBS	Phosphate Buffered Saline

SYMBOLS

ε	Extinction Coefficient

1

MOTIVATION AND OBJECTIVES

Recent worldwide events enhanced the role that biosensing technologies have in medical diagnostics and disease monitoring, resulting in an increase demand for more convenient sensing platforms. Biosensors, such as Point-Of-Care (POC) played a fundamental role in the recently pandemic of COVID-19, where was necessary attain fast results for a large number of persons. However, these tests are far from gold-standard techniques as they suffer from low sensitivity. In order to address this weakness Calorimetric Lateral Flow Assay (C-LFA) has been tested and optimized. It proposes the use of AuNPrs, due to their optical properties, as heat transductors for detecting analytes such as genetic material of virus or bacteria.

In our case, the system was fine-tuned for the detection of the genetic material of the influenza A(H1N1) virus. The samples were pre-incubated for 15 minutes and run in the system also for 15 minutes, following by exposing the test line area to irradiation for results development.

Spiked samples with synthetic DNA were tested in complex matrixes such as virus transport and preservation media from Biocomma and DeltaLab, simulating real samples conditions. In addition, we also simulated a real scenario where real patient samples were used along with the same complex matrixes.

2

INTRODUCTION

2.1 Influenza Virus

Influenza, commonly known as flu, is an infectious disease which affects mainly the respiratory system.[1] Influenza is caused by a group of RNA viruses, Influenza viruses, members of the family *Orthomyxoviridae*.[2] They are classified in four types (influenza A, B, C and D) of which influenza A and B are the most important from a clinical point of view, being the most responsible for outbreaks of seasonal flu in humans. [1]–[3] However, the influenza virus type A it is the one that usually "flow" among humans and, the most common subtypes have been A(H1N1) and A(H3N2). [4]

The subtype A(H1N1), scientifically labelled "A(H1N1) pdm09", has been related to pandemics throughout history. [4] The 1918 "Spanish Flu" can be considered as the deadliest virus in modern history and possible of all time. [5] A highly virulent influenza A (H1N1) virus was responsible for the influenza pandemic that swept across the globe from 1918 to 1919.[5] Studies revealed that the "Spanish Flu" was originated in a bird host (avian influenza or bird flu), so it was considered as zoonotic disease.[4], [5] The total death toll remains uncertain as many places did not maintains medical records, but 20 to 50 million people as estimated to have died, worldwide.[5], [6] In 2009, a new pandemic caused by influenza virus appeared in the United States and quickly spread along the world (Figure 1). [5], [6] It was less contagious and more controlled than "Spanish Flu", but had a significant impact due to the large number of related deaths. [5], [6]

2.1.1 Impact on society

According to the Centres of Disease Control and Prevention the mortality rate for flu in world population is estimated around 0,03% during the Influenza pandemic in 1968, 1% to 3% during the Influenza pandemic in 1918 and between 0,001% to 0,007% during the Influenza pandemic in 2009 (Table 12). [5], [6]

The World Health Organization (WHO) has estimated approximately 3 to 5 million annual epidemics resulting in severe illness, and proximately 290 000 to 650 000 deaths from respiratory causes. [2] Flu severity ranges from mild to severe. In high-risk groups, pregnant women, children under 5 years old, elderly above 65 years old and people with chronical or immunosuppressive conditions, it can lead them to hospitalization and in the worst-case death. [2]

Prevention of new pandemic situations globally is built upon three pillars: prevention, effective and rapid responses. [2] Early detection to make a quick decision is very important. A rapid, fast and inexpensive diagnosis is thus fundamental. Biosensors commonly known as Point of Care (POC) or Rapid Diagnosis Test (RDT) systems, have been developed by researchers around the world to detect viruses and bacteria, giving result between 10 to 15 minutes. However, the sensitivity of these tests is not sufficient when compared with more sophisticated techniques. Beyond RDTs tests, PCR, it is considered a gold standard for the detection of genetic material as it allows to determine the presence of viruses or bacteria with higher precision and sensitivity than other techniques. The main disadvantage is the time for results, it take from one to several hours. [7]–[9]

Despite having lower sensitivity compared to gold standard techniques, RDTs have helped to prevent the spread of diseases. An example is the recent COVID-19 pandemic, where these POC RDTs were fundamental.

2.2 Biosensor

A biosensor is defined as a device combining a biological bioreceptor with a transducer to produce a signal used to identify and/or quantify specific compounds. [10]

2.2.1 Components of a Biosensor

A biosensor, is a device combining three components: a bioreceptor, a transducer, and an electronic system. The latter generally includes a signal amplifier, processor, and display (Figure 2). [10], [11] To perform a detection, the sample to be analysed is placed in contact with the bioreceptor, which interacts with analyte of interest. The signal thus generated goes by the transducer, producing a measurable signal that is proportional to the amount of the analyte in the sample. The signal is processed by the electronic system and shown on the display. [10], [11]

2.2.1.1 Analyte

The analyte or target is a substance, biomolecule, or chemical component, generally present in a sample, which is detected during an assay. Its detection can be generate a range of information such as its concentration, properties, or interactions depending on how the recognition is performed and also how data are processed.[10], [12]
The analyte target considered in this project is the genetic material of Influenza virus subtype A(H1N1).

2.2.1.2 Bioreceptor

The bioreceptor, is a crucial element for the biosensor recognition system and its specificity. Different types of bioreceptors can be used, such as enzymes, antibodies, nucleic acids, aptamers or even whole-cell.[10], [12] It is a centrepiece for a bioreceptor be specifically sensitive towards the desired target-analyte to prevent interference by other substances presents in the sample matrix. [10], [12]
The bioreceptor considered in project is the protein Streptavidin, a tetrameric protein obtained from the *Streptomyces avidinii* bacterium and which binds strongly to Biotin. [13], [14] This binding reaction corresponds to the recognition process, which will be detailed in the following paragraphs. [13], [14]

2.2.1.3 Transducer

The transducer, in general, can be defined as an element that converts one form of energy into another. In a biosensor, this component converts the bio-recognition event into a measurable signal. [10] These signals can be electrochemical (potentiometry, conductimetry, etc.), optical (colorimetry, fluorescence, interferometry, etc.), calorimetric (thermistor, etc.), mass change (piezoelectric, etc.), or magnetic.[15] After the transduction step, the signal needs to be processed and conditioned by the biosensor display to provide specific quantitative or semi-quantitative information. [15]
The transducer considered in this work is the laser which is used to irradiate the gold nanoparticles. Gold nanoprisms have particular optical properties, they exhibit strong absorption In the NIR range and upon light excitation, local solid heating can be generated by the photothermal conversion of the absorbed light energy into local heating.[16], [17] This heat is transferred to a thermosensitive material in which appears a dark spot, If the sample is positive, as consequence of the heat produced. This spot is the test result. [16], [17]

2.2.1.4 Electronics and Display

This component of the biosensor processes the transduced signal in a visual result. Subsequently, it interfaces an user interpretation system to generate an output signal displayed in various formats, including numeric, graphical, tabular, or as an image. [10]

In this work, the display of the optical response obtained due the irradiation of NPrs with NIR light, was a thermosensitive paper.

2.3 Nanomaterials: metallic nanoparticles properties

The interaction between electromagnetic radiation and metallic nanoparticles generates a collective movement of electrons within the nanoparticles in a dielectric medium at a specific resonance frequency causing the excitation of the electrons in their plasmonic band.[16], [18] The phenomenon considered there is called localized surface plasmon resonances (LSPR), and it happens, when the conduction electrons on the metallic nanoparticles are excited by incident light, at the resonant frequency. [16], [18]–[22] Therefore, they can experience heat loss due to interactions with the metal atom lattice, resulting in light absorption or they can experience the displacement of negatively charged free electrons relative to the positively charged metal nucleus. [16], [18]–[22] This charge separation generate an oscillating dipole that emits electromagnetic radiation at the same frequency of oscillation, thus giving rise to phenomena of light scattering. [16], [18]–[22] This phenomenon is explained also in the Figure 3.
Plasmonic nanoparticles are nanoscale metallic particles, sizes ranging from 1 to 100 nanometres, with unique optical properties due their size and shape. [16], [23]The are made of noble metals, such as gold, silver or platinum. These NPs have received notorious attention due to singular properties.[16], [18], [23] Which allows their use in medical applications, such as imaging [24], phototherapy [25], and, more recently in thermal sensors [26].

2.3.1 Types and Shapes of nanoparticles

The LSPR band in noble metal NPs is affected by a combination of several factors such as composition, size, shape and dielectric constant of the medium. These properties and their high biocompatibility and easy surface modification with thiolated molecules makes them very useful in areas such as biomedicine.[16][23]
We have interest in gold nanoparticles (AuNPs), which can be synthetized with a large number of shapes like pseudospheres, rods, triangular prisms,etc. [16], [27], [28]
In pseudospherical NPs the main contribution that affects the position of the LSPR band is their diameter. [16], [29] Pseudospherical NPs with a diameter smaller than 100 nm have a characteristic LSPR band in the visible region of the spectrum, presenting a reddish colour which can be tuned by the NPs's diameter. [16], [29] For anisotropic AuNPs, such as triangular gold nanoprisms, issues such as symmetry and aspect ratio can be tuned to change their optical properties.[16], [29] Figure 4 shows the different colours that can be obtained from AuNPs with different shapes and sizes.

2.3.2 Triangular Gold Nanoprisms (AuNPrs)

Triangular Gold nanoprisms (AuNPrs) are plasmonic anisotropic gold nanoparticles exhibiting strong absorption in the NIR range upon light excitation, caused by edges and tips present in their structure. [16], [17] A strong local heating can be generated in these areas by the photothermal conversion of the absorbed light through a non-radioactive mechanism. [16], [17] These regions act as "hot spots" and are very sensitive to bulk and local dielectric changes, and can be used in a wide area of medical applications. [16], [17]
They presented limitations regarding their production methodologies reproducibility difficult to control. [16], [17] To overcome this problem, researchers proposed to use cationic surfactants such as Cetyltrimethylammonium bromide (CTAB) which present also high toxicity. [16], [17] A methodology has been published to achieve high-yield and reproducible production of gold nanoprisms without using CTAB. [16], [17] This methodology allows obtaining a length of the NPs between 100-170nm and 9nm thickness. [16], [17] These NPrs

obtained showed a surface plasmonic band defined in the near-infrared (NIR) range, demonstrating their compatibility and functionalization ability as photothermal agents [16], [17] The Figure 5 has been obtained from a study comparing the optical properties of two different types of gold nanoparticles: gold rods and gold prims synthesized in two different ways. [30] The prisms were obtained through a surfactant-free methodology, very similar to the one used during the development of this work, while the rods were synthesized using CTAB. The heating efficiency was higher in the latter case, but due to its high toxicity, its use in in-vitro experiments is limited.[30]

2.4 Immuno-Biosensor

An Immuno-biosensor is a type of biosensor that uses components of the immune system, such as antibodies or antigens, as bioreceptors to detect specific biological molecules or pathogens in medical, environmental, or research applications. [31] They harness the specific biding properties of antibodies or antigens to achieve highly selective and sensitive detection. [31] Often, they are enhanced by the incorporation of nanomaterials and they are called Immuno-nanobiosensor. [31] Lateral flow immunoassays (LFIAs) are promising candidates for POC diagnosis. They are easy to use and enable rapid detection without specialized operator or equipment [31]. LFIAs were initially developed in 1959 and gained popularity during the COVID-19 pandemic[17].

The concept explored in this work is the detection of biomolecules by plasmonic heating nanoparticles using a modified LFIA. Particularly it has been applied for the detection of Influenza type A virus. Due the historical impact of the A(H1N1) virus, in our case we have focused in the detection of this specific target. A(H1N1) virus detection tests can be classified in; i) PCR-based test, detecting the virus's genetic material using specific primers, or; ii) rapid tests, which typically detect surface proteins of the virus. PCR-based tests take hours to complete the result, while rapid tests results are obtained in a few minutes and are easy to carry out. The biosensor that has been developed in this work is a paper-based platform tailored from the well-known and widely used LFIAs.[17] A typical LFIA system consists of five components, tightly integrated into a polyvinyl chloride backing card sheet; 1) Sample Pad: where the specimen is applied, serving as the initial point of contact. 2) Conjugate Pad: made of glass fibre, this pad carries the biofunctionalized particles. 3) A nitrocellulose membrane: housing the biomolecules responsible for the test and control lines, crucial for detecting and validating the assay's results. 4) Cellulose Wicking Pad: Specifically designed to facilitate the efficient flow of liquids, this pad ensures a smooth and rapid movement of the sample. 5) A protective film that ensures good contact between the components and safeguards the biomolecules from friction with the system's elements and from humidity. A diagram of the conventional LFIA is in Figure 6.[32]

Here, streptavidin was immobilized on the nitrocellulose membrane. A thermosensitive substrate was included to obtain a thermal response. The recognition event involves Streptavidin-Biotin complex, A(H1N1) and NPrs@oligo.

The biomolecular interactions form the Streptavidin-Biotin complex, biotinylated probes are also used during the biorecognition reaction to detect the analyte of Interest, A(H1N1). The thermal response is obtained through the Incidence of a NIR laser on the AuNPrs, since they will convert light into heat, generating a visible spot on the thermosensitive substrate.

This system pretends to detect rapidly the presence of Influenza virus for ultra-low concentrations trying to solve the adverse effects inherent with the general RDTs tests, such as very weak sensitivity and consequently low LOD. [17] The main advantage of this TLFA is that very low analyte concentrations, between 0,005pmol and 0,0001pmol, which would result in a visual signal not perceptible by the human eye, but could be detected by thermal sensor after the NIR laser irradiation of the test line area. [17]

2.5 Oligonucleotides and oligonucleotide-based Biosensors

Oligonucleotides are short chains of nucleotides, they exhibit remarkable versatility, as they can adopt a wide range of structures apart of the conventional DNA double helix. [33], [34] This property makes them useful in biomedical areas, as therapeutic elements, and also in biotechnology, for biosensing. Oligonucleotides with guanine-rich areas have significant interest due to association formed by oligos with these kinds of regions. [35]–[37] Formations with high value are the triplex structures which are typically formed by adding triplex-forming oligonucleotides, with guanine-rich or polypurine-rich areas, to duplex or single DNAs oligonucleotides, with polypyrimidine-rich areas. [38], [39] Depending on its orientation, different types of triplex structures can be formed: i) the parallel triplex is formed when a polypyrimidine sequence binds in parallel orientation to the polypurine conventional Watson and Crick strand and is stabilized by Hoogsteen hydrogen bonds; ii) the antiparallel triplex form is found when the interaction occurs in the opposite orientation. [35]–[39] They have received great attention not only for the special structures they are capable of forming but also for the speed of formation and low affinity constant when interacting with the detection target.[35]–[39]
Following this methodology, single-stranded oligonucleotides with a central mismatch have been introduced into target cells to repair single-base mutations (Figure 7). [34] In this work, different types of triplexes have been designed, related to different areas within the genetic material of the Influenza virus A(H1N1) subtype, to test which ensured better and stronger capture of the RNA target compared with traditional approaches based on duplex hybrids through linear DNA probes. The functionality of the triplex and duplex formation oligonucleotides was evaluated in our thermal lateral flow biosensor device showing a good correspondence between the theoretical properties of these oligonucleotides and previously reported examples. The detection limits obtained are in the order of nanomolar or lower.

2.6 Methodology of the Biosensor

The Calorimetric Lateral Flow Assay (C-LFA) works with similar procedure and principles than a conventional LFA. The liquid sample containing the analyte to be detected is placed on the sample pad, in which it will be moved by capillarity, on a polymeric strip containing molecules that interact with the analyte (Figure 8). [40]
Conventional LFA, gives a rapid answer for the presence of the specific analyte in the assay sample, C-LFA also allows to determinate the analyte´s concentration with higher sensitivity and specificity. It is based on a paper platform for the detection and quantification of analytes in complex matrixes. [40] The sample is placed in the test device and the result is displayed within 15 minutes.[40] To carry out the assay with the C-LFA system is necessary to mix a small amount of a sample in universal transport or buffer medium, with a suspension of the functionalization AuNPrs (bioconjugate), and the biotinylated probe. The oligonucleotide on the AuNPr interacts with the genetic material of the virus and the biotinylated probe, both in different and distant regions. Biotin included in the capture probe, will interact with the streptavidin deposited on the nitrocellulose membrane, completing the biorecognition.
The mixture is allowed to elute through the membrane for 15 minutes. Then, the casting is introduced into the laser developer where the test line area will be irradiated. After irradiation, the back of the strip where the thermosensitive material is located, is observed. If this material remains intact, we have a negative sample, but if it shows a dark mark, the result is positive. The Figure 8 summarizes the final part of the C-LFA process.

3

METHODS AND MATERIALS

3.1 Synthesis of AuNPrs

The two syntheses of the nanoparticles used in this project were carried out using a protocol already developed and published, [16] for PEG procedure and [41] for Glutathione procedure, only with small modifications. Both syntheses are divided in two phases, first one is the synthesis of NPrs, which is common to both, and the second one is the purification of NPrs, which is what differentiates one synthesis from the other. One of them employs glutathione, a zwitterionic thiol molecule that enhances interparticle interactions, leading to precipitation. This effect is more significant in nanoprisms compared to nanospheres (NSs) because of the larger, flatter surface area of NPrs, which promotes multiple-point interactions. The other method involves treating the synthesized mixture with heterobifunctional thiol-containing PEG to stabilize the nanoparticles, followed by a purification step through electrophoretic separation. Because NSs exhibit higher electrophoretic mobility and small hydrodynamic diameters compared to nanoprisms, the nanospheres migrated into the gel while the NPrs remained in the wells. The protocols with the respective changes are detailed in the annexes (A Protocols).

3.1.1 1st Phase – Synthesis

Laboratory materials: 2 bottles of 1L; 4 beaker of 250 mL; 1 beaker of 500 mL; 2 beakers of 250 mL, 1 beaker of 100 mL; 1 magnet; temperature probe; magnetic stirrer; orbital shaker; addition adapter for peristaltic pump.
Equipment: Peristaltic pump Masterflex (model: 07514-10); Incubator Memmer IPP30; Sonicator Elma sonic P.120H; Precision balance, UV/VIS spectrophotometer Jasco V-670.
Reagents: $Na_2S_2O_3$; $HauCL_4$; KI; aqua regia (caution: highly toxic and corrosive); Fisher water HPLC Gradient grade; Milli-Q water; $NaBH_4$; PEG-5000D (synthesis 1); Glutathione (synthesis 2).

3.1.2 2nd Phase - Purification

3.1.2.1 Purification of AuNPrs for PEG-5000D

Laboratory Materials: 3 Beckman centrifuge tubes; waste container; Erlenmeyer flask.
Equipment: Microwave; Sonicator Elma sonic P.120H; Electrophoresis (source Biosciences EPS 601); Centrifuge (Avanti J-26XPI and motor JLA 16.250); UV/VIS spectrophotometer Jasco V-670; DLS Malvern; SEM.
Reagents: TBE 0.5x; Agarose; Milli-Q water; AuNPrs.

3.1.2.2 PEG Coating and Purification of AuNPrs for Glutathione

Laboratory Materials: 3 Beckman centrifuge tubes; waste container; Erlenmeyer flask.

Equipment: Microwave; Sonicator Elma sonic P.120H; Centrifuge (Avanti J-26XPI and motor JLA 16.250); UV/VIS spectrophotometer Jasco V-670; DLS Malvern; SEM.
Reagents: Glutathione; PEG-5000D; Milli-Q water; $NaBH_4$; Borate buffer 100 and 10 mM pH 8; AuNPrs.

3.2 Biofunctionalization of AuNPrs:

Laboratory Materials: Eppendorf's of 2 mL (low biding Eppendorf); Syring filters of 0.2 microns and 20 mL synriges.
Equipment: Incubator Memmer IPP30; Centrifuge 5427R; Centrifuge (Avanti J-26XPI and motor JLA 16.250); UV/VIS spectrophotometer Jasco V-670; ChemiDoc™ Imaging System
Reagents: MES 10 mM pH6; EDC; Sulfo-NHS; Oligo Duplex-amino; Oligo Triplex-amino; AuNPrs; Milli-Q water; PEG-750D; Hepes 10 mM pH 7.4; MES 50 mM pH 6; Hepes 10 mM pH 7.4 BSA 0.1% T_{20} 0.1%

3.3 Lateral Flow Baking Cards preparation and Assembly

Materials: Chopped glass combined with adhesive Conjugated Pad grade 8964 (Ahlstrom-Munksjö Oyj); Cotton Absorbent Pad grade 222 (Ahlstrom-Munksjö Oyj); Nitrocellulose membrane (FF80HP, Cytiva); Thermosensitive paper; PCR Eppendorf's of 200 µL, 1 500 mL glass bottle and a plastic tray.
Equipment: Guillotine Cutter; XYZ dispenser HM3030; Presser; Incubator Memmer IPP30
Reagents: Streptavidin; Milli-Q water; Boric Acid 50 mM pH 8 BSA 0.5% PVP 0.5% T_{20} 1%.

3.4 Testing Spiked Samples, with synthetic probes, in water or Viral Transport media

During this phase of the project, test strips were run using samples spiked with different concentrations of synthetic DNA probes and nanoparticles biofunctionalized with oligonucleotides forming duplexes and triplexes at various oligonucleotide concentrations, to establish calibration curves. Additionally, various viral transport media have been included.
Laboratory Materials: 96 well testing plate; Eppendorf tubes of 1.5 mL; Clamp.
Equipment: Opus state continuous wave NIR Laser 1064nm
Reagents: PBS10x pH 9; Tris 50 mM pH 9 100 mM NaCl; Tris 50 mM pH 9 100 mM NaCl 50 mM $MgCl_2$; Tris 50 mM pH 9 100 mM NaCl 25 mM $MgCl_2$; Milli-Q water; spiked samples; AuNPrs@oligo; Biocomma (viral transport media); Delta Lab (viral transport); phosphate buffer 10 mM pH 7.4; PBS 1x pH 7.4 BSA 0.5% T_{20} 1%; Hepes 10 mM pH 7.4.

3.5 Testing Real Samples

In the final part of the project, the hospital provided a few real samples in viral transport medium. We did not receive a large quantity of samples that allow for extensive statistical analysis because the case of influenza A have been very low during the 2023 flu season. These real samples were tested on the developing sensor to verify whether the procedures carried out with spiked laboratory samples could be applied to real clinical samples
Laboratory Materials: Samples Box; Eppendorf's of 1.5 mL
Equipment: Opus state continuous wave NIR Laser 1064nm; Sterility test hood.
Reagents: PBS 10x pH 7.4 BSA 0.5 % T_{20} 1%; Milli-Q water; AuNPrs@oligo; Real samples

4

RESULTS AND DISCUSSION

4.1 Synthesis of Triangular Gold Nanoprisms

Gold nanoparticles (NPrs) with a Plasmon Band in the 1000-1200 nm range were synthesized following a modified method from the originals developed by [16] and by [41]. The final protocol used will be described in full detail in the annex. Prior to use, glassware underwent meticulous preparation, including thorough cleaning with aqua regia and rinsing with high-quality Milli-Q water from the EMD Millipore Q-POD® system (Darmstadt, Germany). For easier understanding, was decided to divide the synthesis process into two phases: One for AuNPrs synthesis and a second one for AuNPrs purification. As mentioned in previous paragraphs, two different methodologies were used, both sharing the first stage of the process, the AuNPrs synthesis, and differing in the purification processes. The first one employs gel electrophoresis for purification, and the second one glutathione to promote purification by AuNPrs precipitation. Next, will be discuss the procedure.

4.1.1 Synthesis of AuNPrs@PEG

The preparation of initial solution is common to both syntheses since, as we have mentioned previously, the only difference between them is the final process of particle purification.

4.1.1.1 Preparation of solutions

$Na_2S_2O_3$ 0.5 mM

To prepare a 400 mL of Sodium Thiosulfate 0.5 mM, 23 mg of $Na_2S_2O_3$ were dissolved in 1 ml of ultrapure water. Once dissolved were added to 1L glass bottle previously filled with 400 mL of ultrapure water.

$HAuCl_4$ 2.5 mM

To prepare a 200 mL of Hydrogentetrachloroaurate (III) hydrate 2.5 mM, 169.895 mg of $HAuCl_4$ were dissolved in 1ml of ultrapure water. After dissolving the amount of HAuCl4 it was added to a 1L bottle containing 200 mL of ultrapure water.

KI 0.1M

To prepare a 100µL of potassium iodide 0.1 M, 1.66 mg of KI was dissolved in ultrapure water.

$Na_2S_2O_3$ 0.5 mM / KI 0.1 M: 300 mL of the previously prepared thiosulfate solution were separated from the rest 100 ml, to these 300 ml were added 21.4 microliters of a 0.1 M KI.

4.1.1.2 Synthesis Process

To perform the synthesis all the solutions were cooled at 19 ºC as have been described at the detailed protocol, once cooled, 140 mL of a $Na_2S_2O_3$ 0.5 mM containing KI 0.1 M aqueous solution was slowly added to 200 mL of 2 mM $HAuCl_4 \cdot H_2O$ aqueous solution. This addition is done in 30 seconds by using the pre-adjusted

peristaltic pump. After 4 minutes, another 140 mL of the same $Na_2S_2O_3$ containing KI 0.1M was added. After another 4 minutes, 60 mL of the 0.5 mM $Na_2S_2O_3$ solution was added to the mixture, also in 30 seconds by using the pump. This resulting mixture was left to react at room temperature for an hour, shielded from light by covering it with aluminium film. UV–VIS spectra collected in a range between 200 and 1300 nm (Figure 9), revealed a prominent absorption peak at 1050 nm, corresponding to Gold Nanoprisms, as well as a minor absorption band at 535 nm, indicating the presence of Gold pseudospherical (polyhedral) nanoparticles as by-products, see Table 1.

Abs 1050	1.260492
Abs 535	0.533768
Maximum pick (nm)	1150
Mass of NPrs (mg)	78.24

Table 1 - Information obtain by quantification of the AuNPrs synthesis.

The concentration of Gold Nanoprisms (AuNPrs) was calculated using their LSPR peak absorbance at 1050 nm, applying a conversion factor (ε) of 29 mL mg^{-1} cm^{-1}, determined through combined UV–VIS spectroscopy and ICP analyses. [16] Once we use a dilution factor of ½ is necessary to multiple the value of Abs 1050 and Abs 535 obtained (Figure 9) by 2 to get the real value. In order to get the quantity of NPrs produced we use the equation:

$$Quantity\ of\ AuNPrs\ (m_{AuNPrs}) = \frac{Abs1050 \times V_{Total}}{Optical\ path \times \varepsilon} \qquad (1)$$

$$\Leftrightarrow m_{AuNPrs} = \frac{1.260492 \times 540\ mL}{0.3 \times 29 \frac{mg}{mL \times cm}} \Leftrightarrow m_{AuNPrs} = 78.24\ mg$$

Once the AuNPrs were synthesized and quantified, their surface was protected with a polyethylene glycol molecule. For this purpose, we added an aqueous solution of HS-PEG5000-COOH with a PEG:Au NPrs ratio of 2:1 (in mg, calculated previously) to the nanoprisms solution. HS-PEG5000-COOH was diluted in 1 ml of Milli-Q water, and a specific volume of 10 mg/mL stock solution of $NaBH_4$ was added to achieve a 1:1 molar ratio of PEG to $NaBH_4$. Then was adjusted the pH to 12 by adding 2M aqueous NaOH under gentle mixing, followed by 30 minutes of sonication at 60 ºC and slowly agitation overnight, protecting the reaction to the light with Aluminium foil, to complete the reaction with HS-PEG5000-COOH.

4.1.1.3 Purification of AuNPrs

The aluminium foil covering the bottle during the night was removed, the solution was stirred vigorously and divided into 3 Beckman centrifuge tubes as was described in the protocol. The total volume obtained after 1st centrifugation stage of AuNPrs was 27mL.

After centrifugation in order to quantify the NPrs and NSs we used the UV/VIS spectrophotometer Jasco V-670 using a cuvette with 0.3 of optical path and the conversion factor, $\varepsilon = 35.86 \frac{mg}{mL \times cm}$ calculated by using ICP analyses (Figure 10).

Abs 1050	0.449105
Abs 535	0.134694
Maximum pick (nm)	1062
Concentration of NPrs (mg/mL)	2.087
Mass of NPrs (mg)	56.35

Ratio of $\frac{Abs\ 1050}{Abs\ 535}$	3.33

Table 2 - Information obtain by the 2nd quantification of the synthesis for AuNPrs@PEG.

Using the equation (2) was possible to obtain the concentration of AuNPrs after 1st centrifugation stage.

$$Concentration\ of\ AuNPrs\ (C_{AuNPrs}) = \frac{Abs1050 \times Dilution\ Factor}{Optical\ path \times \varepsilon} \quad (2)$$

$$\Leftrightarrow C_{AuNPrs} = \frac{0.449105 \times 50}{0.3 \times 35.86 \frac{mg}{mL \times cm}} \Leftrightarrow C_{AuNPrs} = 2.087\ mg/mL$$

Since we have the V_{AuNPrs} and c_{AuNPrs}, it´s easy to calculate the quantity of nanoprisms that we got after 1st centrifugation stage, recurring to a basic equation as (3).

$$Concentration\ of\ AuNPrs\ (C_{AuNPrs}) = \frac{mass\ of\ AuNPrs\ (m_{AuNPrs})}{Volume\ of\ AuNPrs\ (V_{AuNPrs})} \quad (3)$$

$$\Leftrightarrow m_{AuNPrs} = C_{AuNPrs} \times V_{AuNPrs} \Leftrightarrow m_{AuNPrs} = 2.087\ mg/mL \times 28.2\ mL \Leftrightarrow m_{AuNPrs} = 56.35\ mg$$

4.1.1.3.1 Agarose at 2.5%

Once we have centrifugated and quantified the nanoparticles the purification process is carried on using an agarose gel. Considering the ratio between Abs 1050 and Abs 535 (Table 2), and since this is bigger than 2.5, we will make the dilution for a 1 mg/mL concentration using TBE 0.5x. So, using the equation (4) is possible to calculate the volume of TBE 0.5x necessary.

$$C'_{initial} V'_{initial} = C_{final} V_{final} \quad (4)$$

$$\Leftrightarrow V_{AuNPrs} = \frac{C'_{AuNPrs} \times V'_{AuNPrs}}{C_{AuNPrs}} \Leftrightarrow V_{AuNPrs} = \frac{2.078 \frac{mg}{mL} \times 27\ mL}{1 \frac{mg}{mL}} \Leftrightarrow V_{AuNPrs} = 56.35\ mL$$

Afterwards, is also necessary to add Glycerol 25% to the solution of AuNPrs as loading reagent. Experi-mentally, it was calculated that the optimal ratio glycerol 25%: AuNPrs was 1:5,6. To perform the calculation was used the equation (5).

$$Volume\ of\ Glycerol\ 25\%\ (V_{Glycerol,25\%}) = 0.18 \times V_{AuNPrs} \quad (5)$$

$$\Leftrightarrow V_{Glycerol,25\%} = 0.18 \times 56.35 \Leftrightarrow V_{Glycerol,25\%} = 10.143\ mL$$

Once diluted and mixed with glycerol, 2 mL of each solution was loaded into a previously prepared agarose gel, 6.15 g of Agarose dissolved by heat with 250 mL of TBE 0.5x, using the microwave. After electrophoresis process, the AuNPrs were removed from the gel (Figure 15), filtrated and prepared for a new centrifugation step at 6000g for 15 minutes. The volume obtained of NPrs@PEG was 3.3 mL. Afterwards, the solution was quantified (Figure 11) and the following results were obtained (Table 3).

Abs 1050	2.38631
Abs 535	0.356605
Maximum pick (nm)	1074

Table 3 - Information obtain by the 3rd quantification of the synthesis for AuNPrs@PEG.

Zeta potential (Table 4) and SEM characterization techniques were used to know how the synthesis process were going on (Figure 16).

Potential Zeta	(-27.3±0.629) mV

Table 4 - Information about the zeta potential of the AuNPrs@PEG

4.1.2 Synthesis of AuNPrs@Glutathione

Similar to the previous protocol the first step, the preparation of solutions was carried out in the same way as before.

4.1.2.1 Preparation of Solutions

$Na_2S_2O_3$ 0.5 mM

To prepare a 400 mL of Sodium Thiosulfate 0.5 mM, 23 mg of $Na_2S_2O_3$ were dissolved in 1 ml of ultrapure water. Once dissolved were added to 1L glass bottle previously filled with 400 mL of ultrapure water.

$HAuCl_4$ 2.5 mM

To prepare a 200 mL of Hydrogentetrachloroaurate (III) hydrate 2.5 mM, 169.895 mg of $HAuCl_4$ were dissolved in 1ml of ultrapure water. After dissolving the amount of $HAuCl_4$ it was added to a 1L bottle containing 200 mL of ultrapure water.

KI 0.1M

To prepare a 100µL of potassium iodide 0.1 M, 1.66 mg of KI was dissolved in ultrapure water.

$Na_2S_2O_3$ 0.5 mM / KI 0.1 M: 300 mL of the previously prepared thiosulfate solution were separated from the rest 100 ml, to these 300 ml were added 21.4 microliters of a 0.1 M KI.

4.1.2.2 Synthesis Process

To carry out this synthesis, we will repeat the steps performed in the first stage of the previously described synthesis 4.1.1.2. The only difference observed was the concentration of the reducing agent, which is slightly higher to adjust the size of the prisms to our maximum requirement by UV. All the solutions were cooled at 19 ºC as have been described at the detailed protocol, once cooled, 140 mL of a $Na_2S_2O_3$ 0.7 mM containing KI 0.1 M aqueous solution was slowly added to 200 mL of 2 mM $HAuCl_4 \bullet H_2O$ aqueous solution. This addition is done in 30 seconds by using the pre-adjusted peristaltic pump. After 4 minutes, another 140 mL of the same $Na_2S_2O_3$ containing KI 0.1 M was added. After another 4 minutes, 60 mL of the 0.7 mM $Na_2S_2O_3$ solution was added to the mixture, also in 30 seconds by using the pump. This resulting mixture was left to react at room temperature for an hour, shielded from light by covering it with aluminium film. UV–VIS spectra collected in a range between 200 and 1300 nm (Figure 12), revealed a prominent absorption peak at 1050 nm, corresponding to Gold Nanoprisms, as well as a minor absorption band at 535 nm, indicating the presence of Gold pseudospherical (polyhedral) nanoparticles as by-products, see Table 5.

Abs 1050	0.950942
Abs 535	0.52025
Maximum pick (nm)	961
Mass of NPrs (mg)	59.024

Table 5 - Information obtained by quantification after the 1st centrifugation stage.

4.1.2.3 Purification of AuNPrs

To purify the Gold Nanoprisms, we employed glutathione, a zwitterionic thiol-containing molecule, which promotes interparticle interactions once conjugation to the gold surface via thiols (SH-) functional groups. This interparticle interactions is more significant in larger particles causing AuNPrs precipitation. For this purpose, we added an aqueous solution of L-Glutathione with a ratio of Gluthatione: AuNPrs 5:1 (in mg, calculated previously) to the nanoprisms solution. L-Glutathione was diluted with 6 mL with buffer solution of borate 10 mM pH 8 and added to the AuNPrs solution diluted with 6 mL with buffer solution of borate 100 mM pH 8. We then adjusted the pH to 12 by adding 2M aqueous NaOH under gentle mixing, followed by static overnight reaction, protecting the reaction to the light with Aluminium foil, to complete the purification

by precipitation. The amount of Glutathione necessary to measure was calculated by using the following equation: $m_{Glutathione} = 5 \times m_{AuNPrs} \Leftrightarrow m_{Glutathione} = 391.2\ mg$.
The following day the supernatant was removed and then added 540 mL of MQ water to resuspend the AuNPrs precipitate. The concentration of Gold Nanoprisms (AuNPrs) was calculated using their LSPR peak absorbance at 1050 nm (Figure 13), applying a conversion factor, $\varepsilon = 29 \frac{mg}{mL \times cm}$ determined through combined UV–VIS spectroscopy and ICP analyses, see Table 6.

Abs 1050	0.708
Abs 535	0.093572
Maximum pick (nm)	1026
Mass of NPrs (mg)	43.944

Table 6 - Information obtained by the 2nd quantification of the AuNPrs synthesis

Since we use a dilution factor of ½ is necessary to multiple the value of Abs 1050 and Abs 535 obtained (Figure 13) by 2 to get the real value. In order to get the quantity of NPrs produced was used the equation (1).

$$m_{AuNPrs} = \frac{0.708 \times 540\ mL}{0.3 \times 29 \frac{mg}{mL \times cm}} \Leftrightarrow m_{AuNPrs} = 43.944\ mg$$

To stabilize the Gold Nanoprisms, we employed heterobifunctional HS-PEG-COOH (Mercapto-ω-carboxy PEG with a molecular weight of 5000 Dalton through conjugation to the gold surface via thiols (SH-) functional groups. For this purpose, we added an aqueous solution of HS-PEG5000-COOH with a PEG:Au NPrs ratio of 2:1 (in mg, calculated previously) to the nanoprisms solution. HS-PEG5000-COOH was diluted in 1 ml of Milli-Q water, and a specific volume of 10 mg/mL stock solution of $NaBH_4$ was added to achieve a 1:1 molar ratio of PEG to $NaBH_4$. We then adjusted the pH to 12 by adding 2M aqueous NaOH under gentle mixing, followed by 30 minutes protecting the reaction to the light with Aluminium foil, to complete the reaction with HS-PEG5000-COOH. The amount of PEG necessary to measure is $m_{PEG} = 2 \times m_{AuNPrs} \Leftrightarrow m_{PEG} = 87.888\ mg$. After the sonication under the described conditions, the solutions were divided in 3 centrifuge tubes and centrifugate as previously mentioned, where was obtained, approximately, 10.5mL of AuNPrs. The final solution obtained was quantified (Figure 14) obtaining the following data (Table 7).

Abs 1050	0.306767
Abs 535	0.0391861
Maximum pick (nm)	1041
Concentration of NPrs (mg/mL)	2.85

Table 7 - Information obtained by the 3rd quantification of the AuNPrs synthesis

Potential Zeta (Table 8) and SEM (Figure 17) was also used to characterize the final AuNPrs obtained.

Potential Zeta	$(-24 \pm 0.990)\ mV$

Table 8 - Information about the quality control of the AuNPrs@Glutathione

4.2 Biofunctionalization of AuNPrs

With the two types of gold nanoprisms that we have prepared previously some functionalizations have been carried out with different types of oligonucleotides at various concentrations, which are detailed below. Two types of oligonucleotides, complementary to different regions of the influenza virus genetic material, were used, Z_2 complementary to region PB1 and Z_8 complementary to the NS one. They are further subdivided into two since the same oligonucleotides were designed with the ability to form duplexes and triplexes: Z_2-Duplex;

Z_8-Duplex; Z_2-Triplex and Z_8-Triplex. In addition was prepared four different concentration for each variation: [1/1] =$1.36 \times 10^{-3} \frac{nmol}{\mu L}$; [1/4] =$3.4 \times 10^{-4} \frac{nmol}{\mu L}$; [1/8] =$1.7 \times 10^{-4} \frac{nmol}{\mu L}$; [1/16] =$8.5 \times 10^{-5} \frac{nmol}{\mu L}$. So, for each type of synthesis, Table 9.

	AuNPrs@PEG				AuNPrs@Glutathione			
DNA	Z_2		Z_8		Z_2		Z_8	
Types of Oligonucleotides	Duplex	Triplex	Duplex	Triplex	Duplex	Triplex	Duplex	Triplex
Concentration (nmol/µL)	[1/1]	[1/1]	[1/1]	[1/1]	[1/1]	[1/1]	[1/1]	[1/1]
	[1/4]	[1/4]	[1/4]	[1/4]	[1/4]	[1/4]	[1/4]	[1/4]
	[1/8]	[1/8]	[1/8]	[1/8]	[1/8]	[1/8]	[1/8]	[1/8]
	[1/16]	[1/16]	[1/16]	[1/16]	[1/16]	[1/16]	[1/16]	[1/16]

Table 9 - Variations of the biofucntionalization done in the AuNPrs considerating the synthesis used.

Previously was necessary to characterize each synthesis to ensure the stability during the storage time (Table 10).

	AuNPrs@PEG	AuNPrs@Glutathione
Abs 1050	0.346092	0.214756
Maximum pick (nm)	1072	1035
Concentration of AuNPrs (mg/mL)	1.61	0.998

Table 10 - Quantification of the AuNPrs different types of syntheses before functionalization.

The biofunctionalization of AuNPrs was performed in two different steps, regardless of whether it is carried out with one type or another of synthesis. Briefly, 250 µg of AuNPrs were reacted at 37 ºC, by shaking, with 500 µl of pre-mixed 1.5 mM EDC and 3.5 mM Sulfo-NHS prepared in 10 mM MES pH 6 during 30 minutes in order to activate the carboxylic groups. After that a washing step by centrifuging 9 min at 6500 rpm and 4°C was performed, then a solution of detection oligonucleotide (Z_2-Duplex; Z_8-Duplex; Z_2-Triplex or Z_8-Triplex) in 50 mM MES pH 6 were incubated with the previously activated AuNPrs for 1.5 h at 37°C. The AuNPrs were then blocked with 500 µl of a solution containing 5% amine-methoxy modified PEG 750 D in 50 mM MES pH 6 for 2h at 37 ºC. Three washing steps were carried out finally and the AuNPRs obtained were resuspended in 10 mM HEPES pH 7.5 containing 0.1% Tween-20 and 0.1 % BSA and stored at 4°C until use. As descripted in the protocol present in the annexes.

4.2.1 Biofunctionalization's confirmation

The procedure used to confirm the successful functionalization involves agarose gel electrophoresis. A 10% agarose gel in 0.5x TBE buffer containing 0.01% GelRed, a DNA intercalator capable of staining both single and double-stranded DNA, was specifically prepared for this purpose. In the gel, 10 µL of the sample mixture is loaded into each well, the procedure to prepare the mix is detailed in the paragraph above. In this was run an aliquot of the oligonucleotide solution before functionalization, as well as an aliquot of the resulting supernatant after functionalization. The discrepancy in the intensities observed in each respective region, upon exposing the gel to a gel viewer, provides insight into the oligonucleotide that has bonded to the prism.
To prepare the sample mix was necessary to centrifuge the DNA aliquots in order to eliminate interferences, especially in the one obtained after functionalization, where there may be traces of gold, which could interfere with the measurements. Once centrifugated and removed 20µL of supernatant the sample mixture was

prepared, the procedure was different if had been functionalized the AuNPrs with triplex formation oligonucleotides or duplex formation oligonucleotides:

Triplex: 4.0µL of sample + 9.3µL of MQ water + 2.7µL of loading solution

Duplex: 5.0µL of sample + 6.1µL of MQ water + 2.2µL of loading solution

The electrophoresis ran at 100V for 35 minutes and after that the gel was observed into the ChemiDocTm Imaging System, see from Figure 22 to Figure 25 which correspond to functionalization using Z_2 Triplex, Z_8 triplex, Z_8 Duplex, and Z_2 Duplex respectively.

4.2.2 Testing for checking and selecting the best synthesis

In order to test the functionalization carried out with the various types of AuNPrs and different concentrations of detection oligonucleotide, four types of prisms were selected for testing using conditions previously developed in the group for similar systems: AuNPrs@PEG with Z_2T [1/1] and Z_8T [1/1]; and AuNPrs@Glutathione with Z_2T [1/1] and Z_8T [1/1].

Stripes with streptavidin at 1 mg/mL in the control and test line and target solutions with concentration of 0.5 pmol in water were prepared. The protocol used is the following detailed: 25µL of target solution was mixed with 10.0µL of biotinylated capture probe, 16.6µL Tris 50 mM pH 9 100 mM NaCl 50 mM $MgCl_2$, 23.4µL running buffer, and 25.0µL AuNPrs solution. The mix was pre-incubated for 15 minutes and then 95.0µL of each sample mix was added into one well of a 96-well plate. The strip was immersed into the sample solution, allowing the liquid to flow through the nitrocellulose for 15 minutes. By last, let the stripes dry in incubation for 30 minutes at 37ºC and observe the results.

The test result was obtained through direct observation of the nitrocellulose membrane, simply by the presence or absence of a signal on the test line. The target concentration is high enough to produce a strong visual signal. The result showed that both samples containing nanoprisms of the synthesis with Glutathione do not have any visual signal on the test line (Figure 18 and Figure 20). On the other hand, the samples containing nanoprims from the syntheses made with PEG showed a visual signal in the test line for both oligonucleotides. Being the visual signal more intense on the test line using the oligonucleotide Z_2T (Figure 19) than the oligonucleotide Z_8T (Figure 21).

Thus, taking into account the results is possible to notice that the best synthesis for this project under the conditions we will work with, is the synthesis of nanoprisms with PEG.

4.3 Calculation of the detection limit (LOD) using spiked samples with synthetic DNA

Once the AuNPrs that will be used during the development of the sensor have been selected, the detection limit, with the nanoparticles biofunctionalized with different amounts of detection probe (Table 9), was determined. The procedure used for this was quite simple; target solutions were prepared ranging from a high concentration that would be visible to the naked eye to a much lower concentration, not visible to the human eye. After running the chromatography lateral flow strip with no visual signal at the test liner were irradiated by using NIR laser. The results were obtained at the back part of the strip, where the thermosensitive material was located.

4.3.1 Calibration Curves

Calibration curves were prepared using AuNPrs funcionalized with different concentrations of oligonucleotide such as [1/1] $\frac{nmol}{\mu L}$; [1/4] $\frac{nmol}{\mu L}$; [1/8] $\frac{nmol}{\mu L}$ and [1/16] $\frac{nmol}{\mu L}$. 10 samples for each calibration curve were prepared in total, ranging from 0 to 0.5 pmol, the lowest concentration used was 0.0001pmol.

The recipe used for the calibration curves was the same one used during the AuNPrs selection, once the lateral flow process was completed, the strips were dried at 37°C before being irradiated using the NIR laser. The irradiation process was carried out for each of the curves after adjusting the working power with the prepared blanks. Once the power was selected, the complete curve was irradiated for LOD determination.

Figure 26 shows an example of one result obtained from the curves performed using a previously optimized protocol for another system. The results obtained for the example shown, Z_2T [1/8], displayed little consistency after the strips were irradiated, which led us to suspect that there might be an issue with the protocol we were using.

4.3.1.1 Optimization of the process

Considering the issues encountered in the previous section, it was decided to try different dilution buffers to see if the problem could be resolved by changing this component of the system. Different combinations were tested (Figure 27):

(A) 25.0µL of target solution + 10.0µL biotinylated capture probe + 16.6µL Tris 50 mM pH 9 100 mM NaCl 50 mM $MgCl_2$ + 23.4µL Fresh PBS 10X pH 7.4 0.5 % BSA 1 % T_{20} + 25.0µL of AuNPrs.

(B) 25.0µL of target solution + 10.0µL biotinylated capture probe + 16.6µL MQwater + 23.4µL Fresh PBS 10X pH 7.4 0.5 % BSA 1 % T_{20} + 25.0µL of AuNPrs.

(C) 25.0µL of target solution + 10.0µL biotinylated capture probe + 16.6µL MQ water + 23.4µL Old PBS 10X pH 7.4 0.5 % BSA 1 % T_{20} + 25.0µL of AuNPrs

(D) 25.0µL of target solution + 10.0µL biotinylated capture probe + 16.6µL Tris 50 mM pH 9 100 mM NaCl 50 mM $MgCl_2$ + 23.4µL Fresh PBS 10X pH 7.4 0.5 % BSA 1 % T_{20} + 25.0µL of AuNPrs.

(E) 25.0µL of target solution + 10.0µL biotinylated capture probe + 16.6µL Tris 50 mM pH 9 100 mM NaCl + 23.4µL Fresh PBS 10X pH 7.4 0.5 % BSA 1 % T_{20} + 25.0µL of AuNPrs.

As observed in the strips shown in Figure 27, the use of $MgCl_2$ had a negative impact on the system. It can be seen in the strips as a white band known as the ghost effect, which caused particle aggregation at the edges of the test line and, consequently, distortion during irradiation, as previously observed. This is known that Magnesium chloride salts has high ionic strength and can cause aggregation of AuNPs even when the concentration is very low [42]. For the following calibration Tris 50mM pH 9 100 mM NaCl will be used as dilution buffer.

4.3.1.2 Optimized Calibration Curves

The preparation of the curves was carried out with the optimizations previously conducted, considering the biofunctionalized AuNPrs shown in Table 9. The target concentration was from 0 to 0.5pmol and the protocol was the same as the one used during the synthesis selection, with the modification introduced in the elution buffer.

All the functionalized AuNPrs were set up at concentration of 400 mg/mL and the irradiation performed after drying the strips at 37 ºC. The optimization of the NIR irradiation was previously done using the blank samples. Irradiation was performed within a power intensity range of 60–70% due to slight variations in AuNPrs concentration. The results at the back part of the strip showed that oligonucleotide Z_2T showed greater sensitivity for low detection oligonucleotide concentrations such as [1/8] (Figure 30) and [1/16] (Figure 31). It was expected to obtain completely the opposite result, higher concentrations of oligonucleotide on the AuNPr would result in greater sensitivity, but this does not occur because high concentrations can also give steric hindrance

in the target-AuNPrs recognition process, leading to decreased sensitivity, see Figure 28 and Figure 29. The sensitivity reached by Z_2T was 0.001pmol for both concentrations, [1/8] (Figure 30) and [1/16] (Figure 31).
On the other hand, the LOD obtained with Z_2D for a concentration of [1/1] (Figure 32) was better than the one calculated with the other concentrations as [1/4] (Figure 33), [1/8] (Figure 34), [1/16] (Figure 35), when irradiated at similar power, but lower than the Z_2T LOD .
The oligonucleotides Z_8T and Z_8D presented aggregation at the test line area which was visible in the example of Figure 36. This aggregation on the test line caused distortions in the irradiation process and for that reason were eliminated for further experiments, see Figure 37.
Despite of Z_2T [1/8] and Z_2T [1/16] having the same sensitivity we will proceed with Z_2T [1/16] once we have the same results with lower quantity of oligonucleotide functionalized into the AuNPrs, consequently producing a cheaper biosensor. So, with the tests was possible to conclude that the oligo Z_2 is more adequate than Z_8 and the triplex formation probe was better than the duplex one. But we will use Z_2D [1/16] as a means of comparison.

4.3.2 Calibration Curves for Viral Transport Media

In addition to performing the curves for LOD calculation in a buffered medium, they were also conducted in viral transport media to closely resemble a test with real samples. Viral transport media are highly complex systems with unknown compositions that can either negatively or positively impact the assay. Two types of viral transport media were selected to receive samples from the hospital such as Biocomma ® and DeltaLab ® transport media (Figure 38).
The results obtained after LOD calculation showed that those matrixes increased the sensitivity of the test which allowed the AuNPrs concentration to decrease from 400 mg/mL to 200 mg/mL in real samples testing.

4.3.2.1 Optimization of the process

For the curves obtaining in viral transport medium, AuNPrs functionalized with Z_2T [1/16] and Z_2D [1/16] were used, with the same protocol that was used for curves in buffered medium. AuNPrs functionalized with Z_2T [1/16] were previously selected as more sensitive, and that's why they will be used in the following experiments. The ones functionalized with Z_2D [1/16] will be used simply to confirm that the sensitivity obtained with these is worse. When the initial tests were conducted using blanks and Deltalab viral transport media, the ghost effect was observed once again in the system (Figure 39). This made us to reoptimize the procedure and test various elution buffers and running buffers. The different types of buffers tested in combinations were: Tris 50 mM pH 9 100 mM NaCl, PBS 1x pH 7.4 BSA 0.5% T_{20} 1%, phosphate buffer 10 mM pH 7.4, Hepes 10 mM and PBS 10x pH 7.4 0.5 % BSA 1 % T_{20}. Was also tested water as elution buffer. However, the results showed the presence of flag effect on the test line for PBS 1x pH 7.4 BSA 0.5% T_{20} 1%, phosphate buffer and Hepes 10 mM, for Z_2T [1/16], and also with PBS 10x pH 7.4 0.5 % BSA 1 % T_{20} for Z_2D [1/16] (Figure 40). Using Mili Q water as dilution buffer and PBS 10x pH 7.4 0.5 % BSA 1 % T_{20} as running buffer no ghost effect was observed (Figure 40). After successfully eliminating the undesired effect in blank samples, we proceeded to prepare highly positive visual samples under the selected conditions, as shown in, Figure 40. These samples were prepared both with and without a 15-minutes pre-incubation period to assess whether preincubation had any impact on the system's sensitivity. It is worth noting that in a separate experiment using a different universal transport medium, pre-incubation was observed to have a detrimental effect on lateral flow. It was demonstrated that the using of pre-incubation with DeltaLab showed also less intensity in comparison when we used non-pre-incubation process.

4.3.2.2 Optimized Calibration Curves

The preparation of the calibration curves was carried out with the new optimizations included and using Z_2T [1/16] and Z_2D [1/16] in Biocomma and Deltalab viral transport media. The target concentration was from 0 to 0.5pmol and the protocol was the same as the one used during the project development, with the modification introduced in the elution buffer.: 25.0µL of target solution + 10.0µL biotinylated capture probe + 16.6µL MQ water + 23.4µL PBS 10X pH 7.4 0.5 % BSA 1 % T_{20} + 25.0µL of AuNPrs at 200 mg/mL. The irradiation was performed after drying the strips at 37 ºC. The optimization of the NIR irradiation was previously done using the blank samples. Irradiation was performed within a power intensity range of 70–80 % due to slight variations in AuNPrs concentration. The results at the back part of the strip, on the thermosensitive paper, showed that AuNPrs functionalized with oligonucleotide Z_2T [1/16], showed a great sensitivity for both virus transport media: In Biocomma the reached LOD was 0.0005pmol (Figure 42) and for DeltaLab of 0.0001pmol (Figure 44).

The AuNPrs functionalized with oligonucleotide Z_2D [1/16] tested with Biocomma universal transport media gave a sensitivity quite lower than the similar triplex formation oligonucleotide 0.001pmol (Figure 43) and it was the same obtained with Deltalab (Figure 45). Surprisingly to us, AuNPrs funcionlized with Z_2D [1/16] tested with Biocomma universal transport media provided acceptable sensitivity, probably because the components of this transport medium favor the recognition of the detection oligonucleotide-target-capture probe, which seemed not to occur in the case of Z_2D [1/16] tested with DeltaLab.

Consequently, it was confirmed that AuNPrs functionalized with lower concentrations of oligonucleotides were not adversely affected by more complex matrices like Biocomma and DeltaLab. In fact, the sensitivity remained acceptable and, in some cases, even increased when compared to calibration curves in buffer media, likely due to an effect stemming from the composition of the transport medium.

4.3.3 Real Samples

At the end of the project, real samples were received and collected only in one of the viral transport media that we had been testing, Deltalab transport medium. The number of received samples was relatively small because the collaborating hospital had not registered a high number of influenza cases during the winter season of 2023.

To check the collected real samples, we used the protocol optimized in previous sections, utilizing AuNPrs functionalized with the Z_2T [1/16] oligonucleotide, as it provided the highest sensitivity during the optimization stages. A minor adjustment was made to the system for testing real samples: strips were used where the components of the lateral flow system were protected with a transparent film and a cassette, Figure 46, and the irradiation was performed without prior sample drying. This was done to closely resemble a commercial test and to keep the testing process as short as possible, in line with the goal of a POC biosensor—to provide quick results for rapid decision-making.

Several control samples were prepared to fine-tune the working parameters, and then the received samples were analysed. There were 5 samples corresponding to positive cases of influenza A, and one of them tested positive for influenza type B, Table 26.

After irradiating the samples, a signal was observed on the thermal paper of all the strips, both for the samples positive for Flu A and Flu B (Figure 47). This could be due to the detection oligonucleotide we are using recognizing common regions in both subtypes of the virus, which is why it may not be 100% specific for Flu A as we had initially expected.

4.3.4 Specificity Tests

When we confirmed that there was some non-specificity with the detection probe being used and that it couldn't distinguish between influenza subtypes, we decided to conduct a specificity assay of the probe in use with different synthetic targets corresponding to various respiratory viruses. These included two targets complementary to two different regions within the genome of the syncytial virus: RSV1 and RSV2, another complementary to a region of the SARS-CoV virus genome, and the corresponding ones for the influenza strains that we have been using since the beginning of the project. The assay was performed using the same protocol that was used for generating the curves, with the target solution being changed for each of the cases. It was prepared highly positive visual samples, 0.5pmol of target in DeltaLab universal transport media and were tested using Z_2T [1/16], Z_8T [1/1] and Z_8D [1/1] at 200 mg/mL. The results obtained at the back part of the strip, on the thermosensitive paper, (Figure 48) showed that the used AuNPrs Z_2T [1/16] were highly specific for the influenza virus. In this assay was also confirmed the aggregation in AuNPrs functionalized with Z_8T and Z_8D (Figure 49), as expected.

5

CONCLUSION AND FUTURE PERSPECTIVES

Two types of AuNPrs synthesis were carried out during the project's development, with differences during the purification process. In the first methodology, purification was achieved through gel electrophoresis after surface protection of the AuNPr with polyethylene glycol, taking advantage of the higher electrophoretic mobility of the spherical nanoparticles obtained as a byproduct. In the second one, we used glutathione, a zwitterionic molecule containing thiol, which promotes interactions between particles once conjugated to the gold surface. These interactions were more pronounced in larger particles, leading the precipitation of AuNPrs. The yield obtained with both methods was very similar, but the second methodology was much easier to perform due to the quicker purification process. Initially, we thought it would be the most suitable for us in the project's development. However, when the different AuNPrs were biofunctionalized with oligonucleotides Z_2T [1/1] and Z_8T [1/1], and checked these prisms on LF strips, by preparing spiked samples with a high concentration of targets to yield a very intense visual signal, was observed that the AuNPrs where glutathione was used as the precipitation-causing element did not display a test line. This could be explained because these AuNPrs with glutathione on their surface, which is a zwitterionic molecule, and also SH-PEG-COOH, which generally is presented in ionic form (negatively charged), conferred to the AuNPrs a very high net negative charge, repelling the negatively charged oligonucleotides used, due to their phosphate groups. This led us to select the AuNPrs@PEG as more suitable for the project's development.

The second decision we made was regarding to the detection probes used to functionalize the AuNPrs. Two probes were designed, one complementary to the PB1 region of the Flu A genome, Z_2, and another complementary to the NS region, Z_8. For both cases, duplex-forming and triplex-forming probes were synthesized, resulting in a total of 4 detection probes. When visual tests were performed with lateral flow systems and prisms functionalized with these probes, we observed that AuNPrs functionalized with Z_8 probes produced a test line in all cases, even in the blanks. This led us to remove these detection probes from our developing sensor, as this aggregation could pose problems when irradiating the samples.

Once the detection probe was selected, we proceeded to optimize the probe concentration used in functionalization to achieve the highest sensitivity. This was done with both Z_2 probes, concluding that the triplex-forming probe provided greater sensitivity, although the duplex-forming probe was also acceptable. The sensitivity obtained improved as the amount of probe bound to the particle decreased. This could be due to potential steric effects during the detection probe-synthetic target recognition process.

Having selected the optimal and most sensitive probe concentration, we moved on to working with viral transport media where real samples could be collected in the future. We worked with two different media and calculated the sensitivity obtained when using the previously selected AuNPrs. After having to re-optimize several system parameters and generating curves, we achieved a fairly good sensitivity for both types of AuNPrs, with a sensitivity of 0.0001pmol for AuNPrs functionalized with Z_2T [1/16] and 0.001pmol for AuNPrs functionalized with Z_2D [1/16].

With the selected AuNPrs functionalized with Z_2T [1/16] and the system methodology fine-tuned for viral transport media, we proceeded to analyse real samples collected from the hospital. Although the collected samples were not numerous, the results obtained using the system under development were quite promising. We were able to differentiate between positive and negative samples within a total time of 20 minutes for all the studied samples.

These results allow us to conclude that a development and optimization process has been carried out for a thermal lateral flow system for the detection of Influenza genetic material in samples with such low genetic material concentrations that they could only be detected using gold standard techniques like PCR. The system will need to be fine-tuned for other transport media, but the preliminary results bode well for the system, as it offers high sensitivity, is fast, easy to use, and can be operated by unskilled personnel using inexpensive equipment. Another advantage worth noting is that coupling this system with lateral flow readers will enable quantitative measurements, aiding clinical decision-making.

6

REFERENCES

[1] Centers for Disease Control and Prevention, "Diagnosing Flu," 2017. [Online]. Available: https://www.cdc.gov/flu/about/qa/testing.htm. [Accessed: 28-Jul-2023].

[2] W. H. Organization, "Influenza (Seasonal)." [Online]. Available: https://www.who.int/news-room/fact-sheets/detail/influenza-(seasonal). [Accessed: 28-Jul-2023].

[3] J. K. Taubenberger and D. M. Morens, "1918 Influenza: The mother of all pandemics," *Emerg. Infect. Dis.*, vol. 12, no. 1, pp. 15–22, 2006, doi: 10.3201/eid1209.05-0979.

[4] C. for D. Co. and Prevention, "Types of Influenza Viruses." [Online]. Available: https://www.cdc.gov/flu/about/viruses/types.htm. [Accessed: 28-Jul-2023].

[5] S. Al Hajjar and K. McIntosh, "The first influenza pandemic of the 21st century," *Ann. Saudi Med.*, vol. 30, no. 1, pp. 1–10, 2010, doi: 10.4103/0256-4947.59365.

[6] L. Vaillant, G. La Ruche, A. Tarantola, and P. Barboza, "Epidemiology of fatal cases associated with pandemic H1N1 influenza 2009.," *Euro Surveill.*, vol. 14, no. 33, pp. 1–6, 2009, doi: 10.2807/ese.14.33.19309-en.

[7] U.S. Department of Health and Human Services, "Influenza Diagnosis," *Centres for Disease Control and Prevention*, 2021. [Online]. Available: https://www.niaid.nih.gov/diseases-conditions/influenza-diagnosis. [Accessed: 28-Jul-2023].

[8] C. for D. C. and Prevention, "Diagnosing Flu." [Online]. Available: https://www.cdc.gov/flu/symptoms/testing.htm. [Accessed: 28-Jul-2023].

[9] P. Berzosa *et al.*, "Comparison of three diagnostic methods (microscopy, RDT, and PCR) for the detection of malaria parasites in representative samples from Equatorial Guinea 11 Medical and Health Sciences 1108 Medical Microbiology," *Malar. J.*, vol. 17, no. 1, pp. 1–12, 2018, doi: 10.1186/s12936-018-2481-4.

[10] N. Bhalla, P. Jolly, N. Formisano, and P. Estrela, "Introduction to biosensors," *Essays Biochem.*, vol. 60, no. 1, pp. 1–8, 2016, doi: 10.1042/EBC20150001.

[11] M. Gonçalves, "Desenvolvimento de um biossensor para rápido diagnóstico da doença de Alzheimer," 2016.

[12] H. Liu, J. Ge, E. Ma, and L. Yang, *Advanced biomaterials for biosensor and theranostics*. Elsevier Inc., 2018.

[13] K. H. Lim, H. Huang, A. Pralle, and S. Park, "Stable, high-affinity streptavidin monomer for protein labeling and monovalent biotin detection," *Biotechnol. Bioeng.*, vol. 110, no. 1, pp. 57–67, 2013, doi: 10.1002/bit.24605.

[14] A. D. Cotton, J. A. Wells, and I. B. Seiple, "Biotin as a Reactive Handle to Selectively Label Proteins and DNA with Small Molecules," *ACS Chem. Biol.*, vol. 17, no. 12, pp. 3270–3275, 2022, doi: 10.1021/acschembio.1c00252.

[15] C. Karunakaran, R. Rajkumar, and K. Bhargava, "Introduction to Biosensors," in *Biosensors and Bioelectronics*, Elsevier, 2015, pp. 1–68.

[16] B. Pelaz, V. Grazu, A. Ibarra, C. Magen, P. Del Pino, and J. M. De La Fuente, "Tailoring the synthesis and heating ability of gold nanoprisms for bioapplications," *Langmuir*, vol. 28, no. 24, pp. 8965–8970, 2012, doi: 10.1021/la204712u.

[17] E. Polo, P. Del Pino, B. Pelaz, V. Grazu, and J. M. De la Fuente, "Plasmonic-driven thermal sensing: Ultralow detection of cancer markers," *Chem. Commun.*, vol. 49, no. 35, pp. 3676–3678, 2013, doi: 10.1039/c3cc39112d.

[18] Y. C. Yeh, B. Creran, and V. M. Rotello, "Gold nanoparticles: Preparation, properties, and applications in bionanotechnology," *Nanoscale*, vol. 4, no. 6, pp. 1871–1880, 2012, doi: 10.1039/c1nr11188d.

[19] A. O. Govorov and H. H. Richardson, "Generating heat with metal nanoparticles," *Nano Today*, vol. 2, no. 1, pp. 30–38, 2007, doi: 10.1016/S1748-0132(07)70017-8.

[20] J. Cao, T. Sun, and K. T. V. Grattan, "Gold nanorod-based localized surface plasmon resonance biosensors: A review," *Sensors Actuators, B Chem.*, vol. 195, pp. 332–351, 2014, doi: 10.1016/j.snb.2014.01.056.

[21] J. S. Fulmore, B. F. Geiger, K. A. Werner, L. L. Talbott, and D. C. Jones, "Feature Article," *Child. Educ.*, vol. 85, no. 5, pp. 293–299, 2009, doi: 10.1080/00094056.2009.10521700.

[22] Rafael Ramírez Jiménez, *Modificación Superficial de Nanopartículas de Oro para Aplicaciones Biotecnológicas*. Zaragoza, 2022.

[23] NanoComposix, "Plasmonic Nanoparticles." [Online]. Available: https://nanocomposix.com/pages/plasmonics#plasmonic-nanoparticles. [Accessed: 29-Jul-2023].

[24] G. Baffou *et al.*, "Thermal Imaging of Nanostructures by," *ACS Nano*, vol. 6, no. 3, pp. 2452–2458, 2012.

[25] E. C. Dreaden, M. A. Mac key, X. Huang, B. Kang, and M. A. El-Sayed, "Beating cancer in multiple ways using nanogold," *Chem. Soc. Rev.*, vol. 40, no. 7, pp. 3391–3404, 2011, doi: 10.1039/c0cs00180e.

[26] Z. Qin, W. C. W. Chan, D. R. Boulware, T. Akkin, E. K. Butler, and J. C. Bischof, "Significantly improved analytical sensitivity of lateral flow immunoassays by using thermal contrast," *Angew. Chemie - Int. Ed.*, vol. 51, no. 18, pp. 4358–4361, 2012, doi: 10.1002/anie.201200997.

[27] Y. Huang, Y. Chen, L. L. Wang, and E. Ringe, "Small morphology variations effects on plasmonic nanoparticle

dimer hotspots," *J. Mater. Chem. C*, vol. 6, no. 36, pp. 9607–9614, 2018, doi: 10.1039/C8TC03556C.
[28] J. Liu *et al.*, "Recent advances of plasmonic nanoparticles and their applications," *Materials (Basel).*, vol. 11, no. 10, 2018, doi: 10.3390/ma11101833.
[29] J. E. Millstone, S. Park, K. L. Shuford, L. Qin, G. C. Schatz, and C. A. Mirkin, "Observation of a quadrupole plasmon mode for a colloidal solution of gold nanoprisms," *J. Am. Chem. Soc.*, vol. 127, no. 15, pp. 5312–5313, 2005, doi: 10.1021/ja043245a.
[30] G. Alfranca, Á. Artiga, G. Stepien, M. Moros, S. G. Mitchell, and J. M. De La Fuente, "Gold nanoprism-nanorod face off: Comparing the heating efficiency, cellular internalization and thermoablation capacity," *Nanomedicine*, vol. 11, no. 22, pp. 2903–2916, 2016, doi: 10.2217/nnm-2016-0257.
[31] J. Zhang and J. Zhao, *Immuno-biosensor*. Elsevier Inc., 2018.
[32] B. Khlebtsov, "Surface-Enhanced Raman Scattering-Based Lateral-Flow Immunoassay," pp. 1–16, 2020.
[33] S. S. Mukrimaa *et al.*, "No 主観的健康感を中心とした在宅高齢者における 健康関連指標に関する共分散構造分析Title," *J. Penelit. Pendidik. Guru Sekol. Dasar*, vol. 6, no. August, p. 128, 2016.
[34] Y. Fichou and C. Férec, "The potential of oligonucleotides for therapeutic applications," *Trends Biotechnol.*, vol. 24, no. 12, pp. 563–570, 2006, doi: 10.1016/j.tibtech.2006.10.003.
[35] C. S. Huertas *et al.*, "Label-free DNA-methylation detection by direct ds-DNA fragment screening using poly-purine hairpins," *Biosens. Bioelectron.*, vol. 120, no. August, pp. 47–54, 2018, doi: 10.1016/j.bios.2018.08.027.
[36] J. F. García *et al.*, "Detection of pyrimidine-rich DNA sequences based on the formation of parallel and antiparallel triplex DNA and fluorescent silver nanoclusters," *Spectrochim. Acta - Part A Mol. Biomol. Spectrosc.*, vol. 297, no. April, 2023, doi: 10.1016/j.saa.2023.122752.
[37] A. Aviñó, R. Eritja, C. J. Ciudad, and V. Noé, "Parallel Clamps and Polypurine Hairpins (PPRH) for Gene Silencing and Triplex-Affinity Capture: Design, Synthesis, and Use," *Curr. Protoc. Nucleic Acid Chem.*, vol. 77, no. 1, 2019, doi: 10.1002/cpnc.78.
[38] A. Aviñó *et al.*, "Detection of SARS-CoV-2 Virus by Triplex Enhanced Nucleic Acid Detection Assay (TENADA)," *Int. J. Mol. Sci.*, vol. 23, no. 23, 2022, doi: 10.3390/ijms232315258.
[39] L. Pla *et al.*, "Triplex hybridization-based nanosystem for the rapid screening of pneumocystis pneumonia in clinical samples," *J. Fungi*, vol. 6, no. 4, pp. 1–14, 2020, doi: 10.3390/jof6040292.
[40] K. M. Koczula and A. Gallotta, "Lateral flow assays," *Essays Biochem.*, vol. 60, no. 1, pp. 111–120, 2016, doi: 10.1042/EBC20150012.
[41] R. Ramírez-Jiménez, Á. Artiga, S. G. Mitchell, R. Martín-Rapún, and J. M. de la Fuente, "Surfactant-free synthesis and scalable purification of triangular gold nanoprisms with low non-specific cellular uptake," *Nanomaterials*, vol. 10, no. 3, pp. 1–10, 2020, doi: 10.3390/nano10030539.
[42] F. L. Heredia, P. J. Resto, and E. I. Parés-Matos, "Fast Adhesion of Gold Nanoparticles (AuNPs) to a Surface Using Starch Hydrogels for Characterization of Biomolecules in Biosensor Applications," *Biosensors*, vol. 10, no. 8, 2020, doi: 10.3390/bios10080099.

A

PROTOCOLS

A.1 Synthesis of AuNPrs

1) Preparation of the material

i. Clean all the material with aqua regia inside of the ventilated hood.
ii. Remove the aqua regia and clean with milli-Q water 5 times.
iii. Label all the material with the respective solutions to being used.

i. Preparation of reagents dilutions in Fisher water

i. 400 mL of $Na_2S_2O_3$ 0.5 mM – measure 32mg of $Na_2S_2O_3$ and dissolve it in 1 mL of Fisher water HPLC Gradient grade. Add this mL to 400 mL of water HPLC grade, in a labelled bottle of 1 L.
ii. 200 mL of $HAuCl_4$ 2.5 mM – measure 169.895 mg of $HauCl_4$ and dissolve it in one 1 mL Fisher water HPLC Gradient grade. Add this mL to 200 mL of water HPLC grade, in a labelled bottle of 1 L.
iii. 100μL of KI 0.1 M – measure 10 mg of KI and dissolve it in one 1 mL of Fisher water HPLC Gradient grade.
iv. Introduce the solutions and material in an incubator at 19ºC for 1h 15 minutes to cool down all the solutions and materials to be used, check the temperature of each solution with a thermometer probe before using.
v. Label the solutions prepared:
    a. Solution S1: 200 mL of $HauCl_4$ 2.5 mM in a bottle of 1L covered with aluminium and with the addition adapter on.
    b. Solution M1: 100 mL of $Na_2S_2O_3$ 0.5 mM in a beaker of 100mL.
    c. Solution M2: 300 mL of $Na_2S_2O_3$ 0.5 mM in a bottle of 1L and add 21.4μL of KI 0.1 M.

ii. Previous adjusts to the peristaltic pump

The pump needs to be adjusted/calibrated before using for each condition to ensure that all volumes will be dispensed in the 30 seconds, specified by the protocol.

2) Synthesis

i. Remove the solution M2 from the incubator and add 140 mL to a beaker of 250 mL. Add this 140 mL to the $HAuCl_4$ solution which is inside the incubator using the calibrated pump, in 30 seconds. Wait 4 minutes before the next addition.
ii. Again, remove the solution M2 from the incubator and add 140 mL to a beaker of 250 mL. Add this 140 mL to the $HAuCl_4$ solution which is inside the incubator using the calibrated pump, in 30 seconds. Wait 4 minutes before the next addition.
iii. Remove the solution M1 from the incubator and add 60 mL to a beaker of 250 mL. Add this 60 mL to the $HAuCl_4$ solution which is inside the incubator using the calibrated pump, in 30 seconds. Allow

the reaction to stand for one hour at 19 ºC protecting it from light with aluminium foil. After 1 hour a quantification step has to be carried out using UV/VIS spectrophotometer Jasco V-670.

iv. Quantification of the synthesis due to the UV/VIS spectrophotometer Jasco V-670.

3) PEG Coating of AuNPrs

i. Measure a quantity of PEG-5000D using the ratio 1:2 (AuNPs: PEG) and dissolve it in 2 mL of MQ water.

ii. Measure 10 mg of $NaBH_4$ and dissolve it in 1mL of MQ water.

iii. Add the same molar quantity of NaBH4 of PEG to the PEG solution. Add this solution to the AuNPrs, during this addition process the solution should be in agitation.

iv. Adjust the pH to 12 using NaOH 2.5M.

v. Insert the bottle in the ultrasonic bath (Elma sonic P.120H) for 30 minutes at 60ºC with the following conditions:
   a. Frequency: 37 KHz
   b. Power: 100%

vi. Leave the reaction agitating overnight at room temperature protecting it from light.

4) Purification of AuNPrs@PEG

i. Divide the AuNPrs@PEG solution in 3 Beckman centrifuge tubes.

ii. Perform 3 centrifugations of 15 minutes at 6500 G and 25ºC.

iii. Quantify the AuNPrs@PEG once finished the centrifugation steps. Check the ratio Abs1050: Abs 535. If the ratio is lower than 2.5 the concentration of AuNPrs@PEG has to be of 1.5 mg/mL, if the ratio is higher than 2.5, the concentration has to be of 1 mg/mL.

iv. Add glycerol 25% to the AuNPrs solution with TBE 0.5x using the ratio 5.6:1 (AuNPrs:Glycerol 25%).

v. Measure 6.15g of Agarose and dissolve it in 250 mL TBE 0.5x using the microwave.

vi. Once the agarose is dissolved, prepare the gel base and place the accessories to create the wells. After they are positioned, carefully add the agarose and let it gel in cold conditions.

vii. Remove the accessories and introduce the gel in the electrophoresis container, then fill the container with TBE 0.5x.

viii. Fill each well of the gel with 2 mL of AuNPrs@PEG solution.

ix. Close the container, turn on the electrophoresis equipment and let it run for 40 mins at 120 V.

x. Remove the purified AuNPrs@PEG from the gaps, green solution.

xi. Divide the AuNPrs@PEG solution in 3 Beckman centrifuge tubes. Perform 3 centrifugations of 15 minutes at 6500 G and 25ºC.

xii. Quantification of purified AuNPrs@PEG solution by using the absorbance at 1050 nm after the centrifugation steps.

xiii. Dilute the purified AuNPrs@PEG with MQ water to a final concentration of 1.5 mg/mL.

xiv. Quality control: prepare a sample for DLS and SEM.

5) Purification of AuNPrs by using Glutathione solution

i. The steps 1), 2) and 3) are repeated in this methodology. Once the unprotected AuNPrs are characterized and quantified, it is necessary calculate the quantity of Glutathione necessary by using the ratio 1:5 (AuNPrs: Glutathione) and dissolved with Borate buffer solution 10 mM pH 8.

ii. Add 60 mL of Buffer solution of Borate Buffer 100 mM pH 8 to the AuNPrs solution.

iii. Add 60 mL of Buffer solution of Borate Buffer 100 mM pH 8 to the AuNPrs solution.

iv. Add the Glutathione dissolved carefully.

v. Adjust the pH to 12 with NaOH 2.5M.
vi. Allow the reaction to stand overnight protecting it from light with aluminium foil.
vii. Remove the supernatant of the solution of AuNPrs@Glutathione.
viii. Add 540 mL of MQ water and mix it.
ix. Quantification of purified AuNPrs@Glutathione solution by using the absorbance at 1050 nm.

6) PEG coating of AuNPrs@Glutathione

i. Calculate the quantity of PEG-5000D using the ratio 1:2 (AuNPrs: PEG) and dissolve it in 2 mL of MQ water
ii. Measure 10 mg of NaBH4 and dissolve it in 1 mL of MQ water.
iii. Add the same molar quantity of NaBH4 of PEG to the PEG solution. Add this solution to the AuNPrs@Glutathione solution, during this addition process the solution should be in agitation.
iv. Adjust the pH to 12 using NaOH 2.5M.
v. Insert the bottle in the ultrasonic bath (Elma sonic P.120H) for 30 minutes at 60ºC with the following conditions:
    a. Frequency: 37 KHz
    b. Power: 100%
vi. Divide the AuNPrs@Glutathione solution in 3 Beckman centrifuge tubes. Perform 3 centrifugations of 15 minutes at 6500 G and 25ºC.
vii. Quantification of purified AuNPrs@Glutathione solution by using the absorbance at 1050 nm after the centrifugation steps.
viii. Dilute the purified AuNPrs@Glutathione with MQ water to a final concentration of 1.5 mg/mL.
ix. Quality control: prepare a sample for DLS and SEM.

A.2 Biofunctionalization Of AuNPrs: AuNPrs@PEG and AuNPrs@Gluthathione

i. Sonicate the stock of AuNPrs and quantification.
ii. Dilute an aliquot of AuNPrs stock to 0.5 mg/mL with MES 10 mM pH6. Add 500 µL of this solution in each Eppendorf tube (low biding).
iii. Measure 2.28 mg of EDC 3×10^{-3} M in 1.5 mL of MES 10 mM pH 6.
iv. Measure 0.69 mg of Sulfo-NHS 7×10^{-3}M in 1.5 mL of MES 10 mM pH 6.
v. Mix the same volume of EDC and Sulfo-NHS and incubate it for 3 mins.
vi. Put 500 µL of that solution in each AuNPrs dilution Eppendorf tube.
vii. Incubate for 30 minutes at 37ºC and with agitation at 170 rpm.
viii. Centrifuge 9 minutes at 6500 rpm and 4ºC
ix. Remove the 950 mL of supernatant.
x. Preparation of the solutions of oligonucleotides Z_2 or Z_8 for different concentration: [1/1] $=1.36\times10^{-3}\,\frac{nmol}{\mu L}$; [1/4] $=3.4\times10^{-4}\,\frac{nmol}{\mu L}$; [1/8] $=1.7\times10^{-4}\,\frac{nmol}{\mu L}$; [1/16] $=8.5\times10^{-5}\,\frac{nmol}{\mu L}$; in MES 50 mM pH 6.
    a. Preparation of oligonucleotides solutions:

Stock of oligonucleotides: [Z_2T] = $0.136\frac{nmol}{\mu L}$; [Z_2D] = $0.0879\,\frac{nmol}{\mu L}$; [$Z_8$D] = $0.114\,\frac{nmol}{\mu L}$; [$Z_8$T] =$0.361\,\frac{nmol}{\mu L}$.

$$[1/16] = 8.5\times10^{-5}\,\frac{nmol}{\mu L} \rightarrow V_{total}(\mu L)\times\frac{8.5\times10^{-5}}{1.7\times10^{-4}} = V'^{1}\mu L\ of\ [1/8] + V'^{2}\ \mu L\ of\ MES\ 50\ mM$$

$$[1/8] = 1.7 \times 10^{-4} \frac{nmol}{\mu L} \rightarrow V_{total}(\mu L) \times \frac{1.7 \times 10^{-4}}{3.4 \times 10^{-4}} = V'^{1} \mu L\ of\ [1/4] + V'^{2}\ \mu L\ of\ MES\ 50\ mM$$

$$[1/4] = 3.4 \times 10^{-4} \frac{nmol}{\mu L} \rightarrow V_{total}(\mu L) \times \frac{3.4 \times 10^{-4}}{1.36 \times 10^{-3}} = V'^{1}\ \mu L\ of\ [1/1] + V'^{2}\ \mu L\ of\ MES\ 50\ mM$$

$$[1/1] = 1.36 \times 10^{-3} \frac{nmol}{\mu L} \rightarrow V_{total}(\mu L) \times \frac{1.36 \times 10^{-3}}{[Stock]} = V'^{1} \mu L\ of\ [Stock] + V'^{2}\ \mu L\ of\ MES\ 50\ mM$$

Where V_{total} Is the total volume necessary for each solution, V'^{1} Is the value of the calculation and V'^{2} Is the difference between V_{total} and V'^{1}.

xi. Add 500 µL to each Eppendorf and mix it.
xii. Incubation for 1 hour and 30 minutes at 37ºC and 170 rpm.
xiii. Remove 20µL of each Eppendorf for characterization.
xiv. Prepare a solution of 5% of amine-methoxy modified PEG-750D in MES 50 mM pH 6, as a blocking agent, add 500 µL to each Eppendorf and mix it.
xv. Incubate for 2 hours at 37ºC with agitation at 170 rpm.
xvi. Centrifuge 4 times for 9 minutes at 6500 rpm and 4ºC:
    a. 1st centrifugation is directly after the incubator
    b. 2nd centrifugation: remove 950 mL of supernatant and add 950 mL of MES 50 mM pH 6.
    c. 3rd and 4th centrifugations: remove 950 mL of supernatant and add 950 mL of Hepes 10 mM pH 7.4.
xvii. After the last centrifugation, the pellet was dispersed in 200 mL of Hepes 10 mM pH 7.4 BSA 0.1% T_{20} 0,1%.

1) Characterization of the AuNPrs biofunctionalization

i. Centrifugate the 20µL sample aliquots collected in the previous xiii. step at 14.5 rpm for 15 minutes.
ii. Remove the supernatant.
iii. Prepare the base for the gel. Place the comb to create the gel wells.
iv. Prepare the agarose gel by measuring 5 g of agarose in 50 mL of TBE 0.5x and dissolve it using the microwave.
v. Once dissolved and cooled add 5µL of Gel Red, mix it and add the mix to the gel support. Let it gelify for an hour.
vi. Meanwhile prepare the sample loading solutions for the gel:
    a. Duplex: 5.0µL of sample + 6.1µL of MQ water + 2.2µL of loading solution
    b. Triplex: 4.0µL of sample + 9.3µL of MQ water + 2.7µL of loading solution
vii. Remove the comb, introduce the gel in the electrophoresis container, and fill it with TBE 0.5x.
viii. Fill the well with 10µL of sample loading solution.
ix. Close the container, turn on the electrophoresis equipment, and let it run for 35 mins at 100 V.
x. Remove the gel and check it by using the ChemiDoc™ Imageging System.

A.3 Lateral Flow Baking Cards Preparation and Assembly

i. Cut the Conjugate Pad and the Absolvent Pad with dimensions of 31 cm length and 3.2 cm width.
ii. Carefully cut the nitrocellulose membrane with dimensions of 31 cm length and 2 cm width.
iii. Cut the thermosensitive paper with dimensions of 31 cm length and 2 cm width.
iv. Prepare a solution of Boric Acid 50 mM pH 8 containing 0.5 % PVP, 0.5 % BSA and 1% T_{20} for Conjugated Pad treatment.

v. Immerse the Conjugated Pad in the treatment solution for 15 mins.
vi. Remove the liquid and let it dry in the incubator at 37ºC.
vii. Stick the nitrocellulose, the treated conjugate Pad and untreated Absorbent Pad at the baking card support.
viii. Laminate the contact areas between components using a laminator, with pre-specified coordinates for applying pressure, for 5 minutes in each zone.
ix. Stick the thermosensitive paper on the back part of the backing card aligning it with the area where the nitrocellulose membrane was located.
x. Prepare the streptavidin solution: quantify the streptavidin stock by UV/ Vis spectra (280 nm) and dilute it at 1 mg/mL in water.
xi. Insert the solution of streptavidin at 1 mg/mL in the XYZ dispenser HM3030 and apply it on the nitrocellulose membrane, where specific coordinates have been predetermined at the equipment for depositing the test line and the control line.
xii. Let it dry in the incubator at 37 ºC for 1 hour.
xiii. Cute by using the guillotine cutter at 0.4 cm width.

A.4 Lateral Flow Assay Procedures

1) Spiked samples, with synthethic probes, in water or Transport media preparation

i. Prepare solutions of synthetic DNA oligonucleotides (target) at different concentrations: 0.5pmol; 0.1pmol; 0.01pmol; 0.005pmol; 0.001pmol; 0.0005pmol and 0.0001pmol from the stock concentration.
   a. Stock 1: concentration 0.5pmol/100µL.
   b. Stock 2: 2µL of stock 1 + 498µL of MQ water
   c. Stock 3: 25µL of stock 2 + 975µL of MQ water
   d. Oligonucleotide Z_2: 0.5pmol solution = $\frac{500\mu L \times 0.02\frac{pmol}{\mu L}}{0.0434\frac{pmol}{\mu L}} = 230\mu L \text{ of stock } 3 + 270\mu L \text{ of MQ water}$
   e. Oligonucleotide Z_8: 0.5pmol solution = $\frac{500\mu L \times 0.02\frac{pmol}{\mu L}}{0.0361\frac{pmol}{\mu L}} = 277\mu L \text{ of stock } 3 + 223\mu L \text{ of MQ water}$

ii. Serial dilutions preparation:
   a. 0.1pmol: 38µL of 0.5pmol + 152µL of MQ water or Universal Virus Transport Media.
   b. 0.01pmol: 26.6µL of 0.1pmol + 239.4µL of MQ water or Universal Virus Transport Media.
   c. 0.005pmol: 106µL of 0.01pmol + 106µL of MQ water or Universal Virus Transport Media.
   d. 0.001pmol: 50.4µL of 0.005pmol + 201.6µL of MQ water Universal Virus Transport Media.
   e. 0.0005pmol: 96µL of 0.001pmol + 96µL of MQ water or Universal Virus Transport Media.
   f. 0.0001pmol: 32µL of 0.0005pmol + 128µL of MQ water or Universal Virus Transport Media.

iii. Running, dilution buffers, and capture probes preparation: Running and elution buffers preparation will be detailed in section **A.5**; Capture biotinylated Stock 3 solution was prepared following the protocol:
   a. Stock 1: Dissolve the original lyophilized product directly in MQ water, following the manufacturer's instructions.

b. Stock 2: 2µL of stock 1 + 498µL of MQ water
c. Stock 3: 25µL of stock 2 + 975µL of MQ water

2) Lateral Flow Assay Procedure

i. Label each Eppendorf tube with the different concentration solutions.
ii. Add in each mixture tube: 25.0µL of the sample solution + 10.0µL biotinylated capture probe Stock 3 + 16.6µL of elution buffer + 23.4µL of Running Buffer + 25.0µL of AuNPrs solution.
iii. Pre-incubate the mixture for 15 mins, if it is necessary.
iv. 95.0µL of each sample mix was added into one well of a 96-well plate. Then introduce the strip and leave the solution flow by capillarity for 15 minutes.
v. Afterward, remove the conjugated Pad and let it dry for 30 mins.
vi. Irradiate the test line area, no visible, with the NIR laser 1064 nm**.**

A.5 Buffers used

Solution	Preparation	Volume (mL)
Aqua regia	75% of the total volume of HCl + 25% of the total volume of HNO_3	1000
Boric acid 0.2M pH 8 (**Stock**)	6.18g of boric acid + 500 mL of MQ water	500
Buffer For Treatment of Conjugated Pad (Boric acid 50 mM pH 8)	BSA 0.5% (2.5g) + PVP 0.5% (2.5g) + T_{20} 1% (5 mL) + 125 mL of Boric acid 0.2M pH8 + 325 mL of MQ water	500
TBE 5x pH 8 (**stock**)	54g of Tris + 27.5g of boric acid 0.2M pH 8 + 20mL EDTA 0.5M + 1980 of MQ water	1000
TBE 0.5x pH 8	200mL of TBE 5x pH 8 + 1800mL of MQ water	2000
Borato Buffer 100mM pH 8	50mL of boric acid 0.2M pH 8 + 50 mL of MQ water	100
Borato Buffer 10mM pH 8	10mL of boric acid 0.2M pH 8 + 90 mL of MQ water	100
MES 100 mM (**stock**)	10.66g of MES + 500mL	500
MES 50 mM	50mL of MES 100 mM + 50mL of MQ water	100
MES 10 mM	10mL of MES 100 mM + 90mL of MQ water	100
Tris 50mM pH 9 (**stock**)	3.03g of Tris + 500 mL of MQ water	500
Tris 50mM pH 9 100mM NaCl	0.584g of NaCl + 100mL of Tris 50mM pH 9	100
Tris 50mM pH 9 100mM NaCl 50 mM $MgCl_2$	0.584g of NaCl + 1.016g of $MgCl_2$ + 100mL of Tris 50mM pH 9	100
Hepes 100mM pH 7.4 (**stock**)	11.92g of Hepes + 500 mL of MQ water	500
Hepes 10mM pH 7.4	10mL of Hepes 100mM pH 7.4 + 90mL of MQ water	100
Hepes 100mM pH 7.4 BSA 0.1% T_{20} 0.1%	10mL of Hepes 100mM pH 7.4 + 90mL of MQ water + 0.5g of BSA +1mL of T_{20}	100
PBS 10x pH7.4 BSA 0.5% T_{20} 1%	9.55g of PBS + 0.5g of BSA + 1mL of T_{20} + 100mL of MQ water	100
PBS 1x pH 7.4 BSA 0.5% T_{20} 1%	0.955g of PBS + 0.5g of BSA + 1mL of T_{20} + 100mL of MQ water	100

Sodium phosphate Monobasic (**stock**; MW: 119.98 g/mol)	6.9g of Sodium phosphate Monobasic + 500mL of MQ water	500
Sodium phosphate Dibasic (**stock**; MW: 141.96 g/mol)	13.4g of Sodium phosphate Dibasic + 500mL of MQ water	500
Phosphate buffer 10 mM pH 7.4	39 mL of Sodium phosphate Monobasic + 61mL of Sodium phosphate Dibasic +100mL of MQ water	200

Table 11 - Method of how prepared the utilized solutions

A.6 Commercial suppliers of the materials used during the project

Potassium iodide (KI; MW: 166.01g/mol), Magnesium chloride hexahydrate ($MgCl_2 \cdot 6H_2O$; 95.21 g/mol), TRIS (MW: 121.14 g/mol), 99% sodium chloride (NaCl; MW: 58.44 g/mol), Tween® 20 (T_{20}; MW: 1228 g/mol), EDTA (MW: 292.24 g/mol), 96% sulfuric acid (H_2SO_4; MW: 98.08 g/mol), 33% hydrogen peroxide (H_2O_2; MW: 34.01 g/mol), 37% hydrochloric acid (HCl; MW: 36.46 g/mol), 65% nitric acid (HNO_3; MW: 63.01 g/mol), MES (MW: 213.26 g/mol), absolute ethanol (C_2H_6O; MW: 46.07 g/mol), sodium thiosulfate ($Na_2S_2O_3 \cdot 5H_2O$; MW: 158.11 g/mol) were purchased from Panreac®.
PEG-5000D and PEG-750D was acquired from Rapp Polymere.
MES was obtained from Alpha Aesar. Chloroauric acid ($HAuCl_4 \cdot xH_2O$; MW: 339.79 g/mol) was purchased from Strem Chemicals.
Sodium hydroxide (NaOH; MW: 40 g/mol), sodium borohydride 98% ($NaBH_4$; MW: 37.93 g/mol), sodium tetraborate decahydrate ($Na_2B_4O_7 \cdot 10H_2O$; MW: 381.37 g/mol), sulfo-NHS (MW: 115.10 g/mol), and EDC (MW: 155.24 g/mol), Boric acid (MW: 61.83 g/mol), BSA (MW: 66430.3 g/mol), PVP-40 (MW: 111.14 g/mol), HEPES (99.5%) (MW: 238.30 g/mol) were obtained from Sigma-Aldrich and used as received.
The agarose was purchased from Lonza. PBS Powder from Ibian Technologies and the oligonucleotides from Biomers.
The LFIA strips used consisted of five parts hold together over a polyvinyl chloride (PVC) backing card sheet obtained from, Kenosha, Switzerland, The Netherlands, with an initial geometry of 80 mm x 300 mm: a glass fiber sample pad grade 8964 from Ahlstrom-Munksjö, Helsinki, Finland which was used also as conjugate pad, a nitrocellulose membrane purchased from FF80HP, GE Healthcare Life Sciences, UK, a cellulose absorption pad 222, Ahlstrom-Munksjö, Helsinki, Finland and in some cases a transparent pro-tected film obtained also from Kenosha, Switzerland.

B

FIGURES AND TABLES

A.7 Introduction

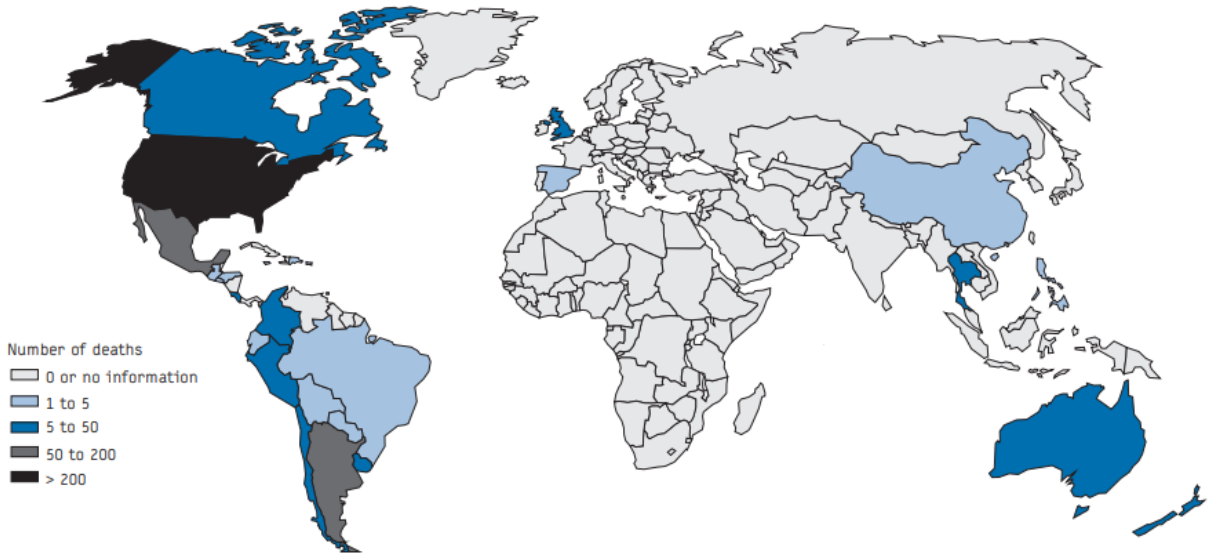

Figure 1 - Deaths associated with pandemic H1N1 influenza 2009 reported officially worldwide as of 16 July 2009.Reproduced [5]. Copyright 2016, Eurosurveillance: bulletin européen sur les maladies transmissibles = European communicable disease bulletin.

Date	Strain	Estimate number of worldwide deaths	Comments
1918-1919 (Spanish Flu)	H1N1	Over 50 million	Three waves: A first, mild wave in the spring of 1918 was replaced by a second wave in September to November, 1918 that resulted in a mortality rate of over 2.5%. A third wave with equally high mortality rates swept around the world in 1919. The virus probably originated from the United States and then spread to Europe.
1957-1958 (Asian Flu)	H2N2	1-1.5 million	Two waves: The virus originated in Southern China in February 1957 and spread over 3 months to Singapore, Hong Kong and Japan and in October 1957 reached the United Kingdom and United States. A second wave was detected in January 1958.
1968-1969 (Hong Kong Flu)	H3N2	¾ million	Two waves in the winters of 1968-1969 and 1969-1970. The virus originated from Hong Kong in July 1968.

Table 12 - Influenza pandemic of the 20th century. Reproduced [6]. Copyright 2016, Annals of Saudi Medicine.

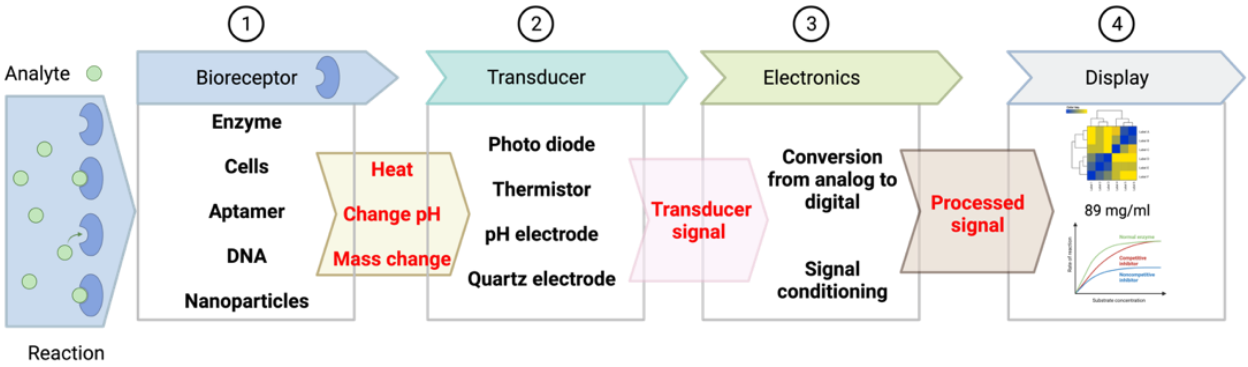

Figure 2 - Schematic representation of a biossensor. Adapted from [10] Copyright 2016, Essays in Biochemistry.

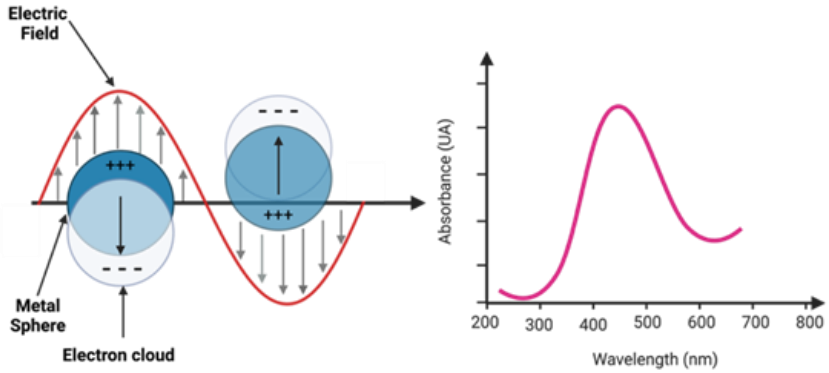

Figure 3 - Schematic illustration of LSPR excitation for spherical nanoparticle. Modified from [19]. Copyright 2016, Sensors and Actuators, B: Chemical.

Figure 4 - Illustration of different gold nanoparticles synthetized in BioNANOSurf laboratory with different size, shape and consequently different LSPR and optical properties.

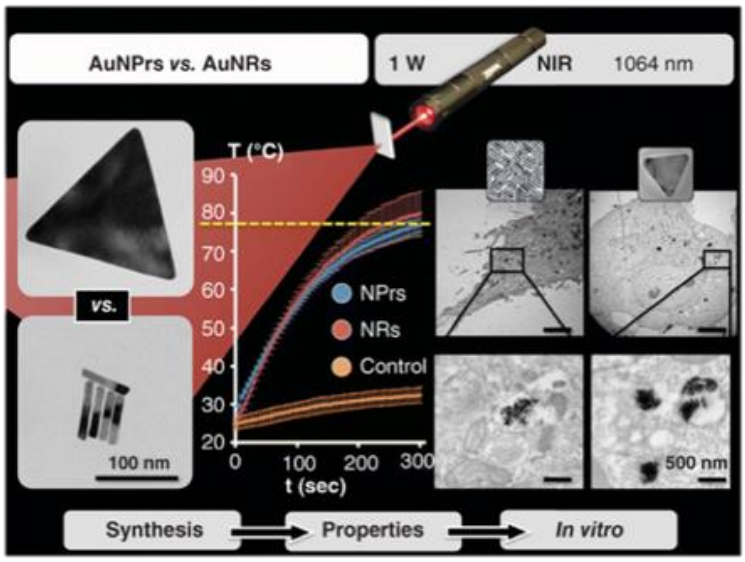

Figure 5 - Illustration with comparative Analysis of Gold Nanoparticles for Enhanced Photothermal Therapy, exploring the diverse properties of Gold Nanorods and Gold Nanoprisms synthesized through varied methods, sizes, and shapes. Reproduced from [30]. Copyright 2016, Nanomedicine.

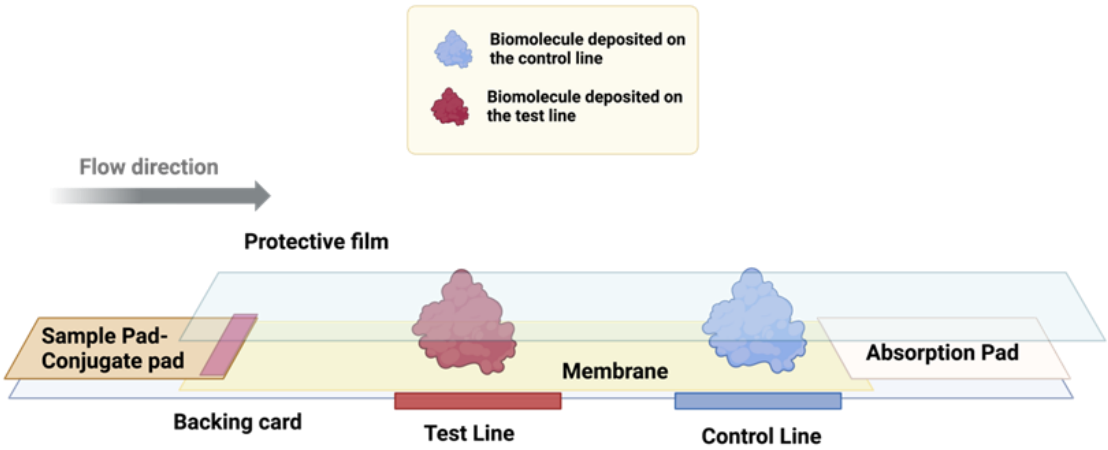

Figure 6 - Typical configuration of a lateral Flow Assay (LFA). Adapted from [40]. Copyright 2016, Essays Biochemistry.

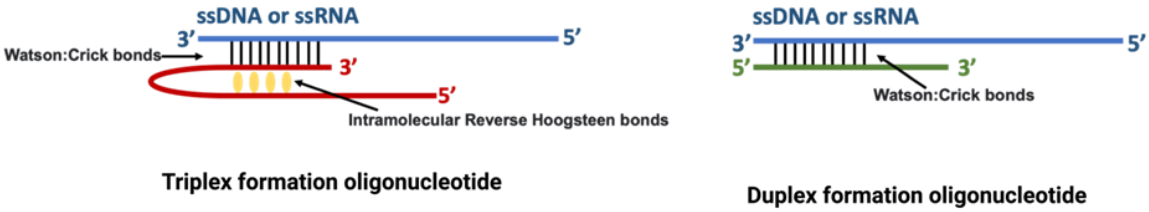

Figure 7 - Comparison of the mechanism for triplex and duplex formation oligonucleotides. Adapted from [36]. Copyright 2016, Spectrochimica Acta - Part A: Molecular and Biomolecular Spectroscopy

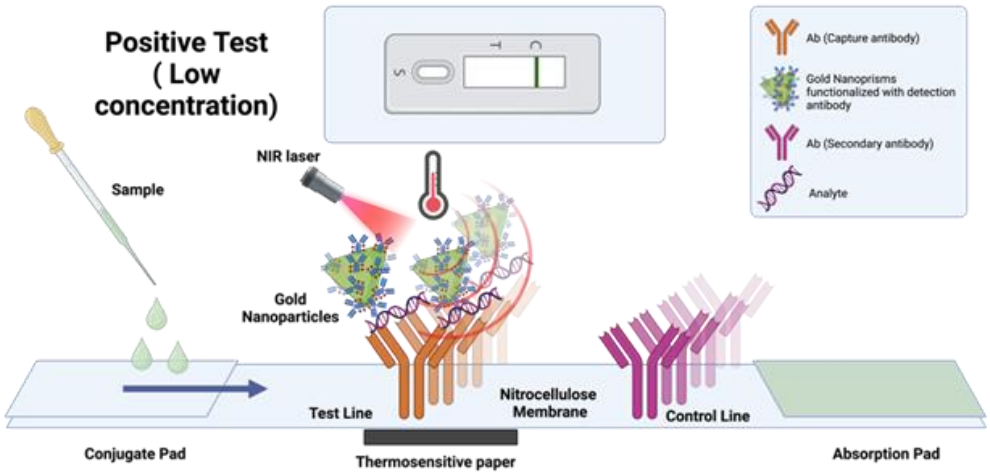

Figure 8 - Schematic representation of a calorimetric thermal lateral flow assay. Adapted from [17]. Copyright 2016, Chemical Communications.

A.8 Synthesis of Triangular Gold Nanoparticles

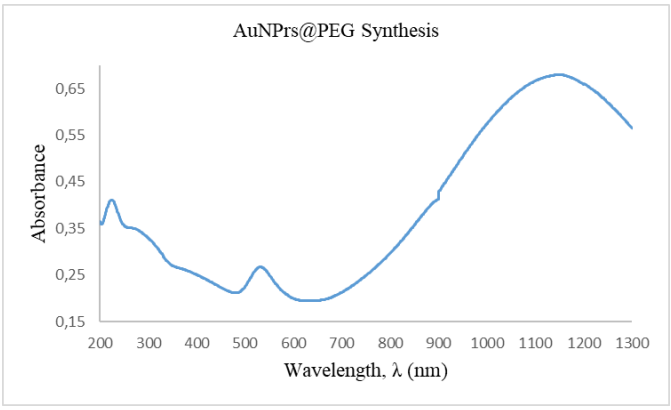

Figure 9 - 1st quantification of the synthesis for AuNPrs@PEG by UV-VIS spectroscopy.

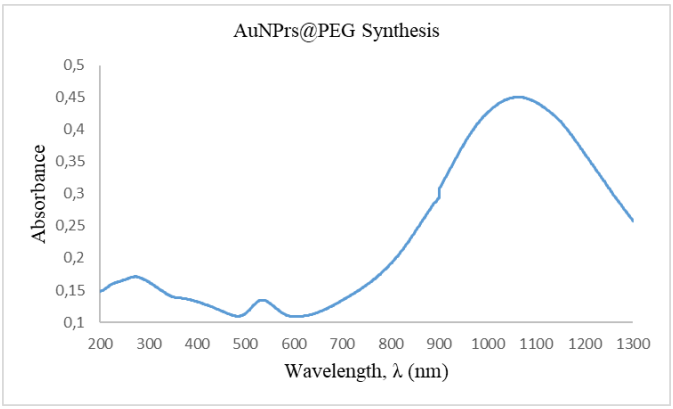

Figure 10 - 2nd quantification of the synthesis for AuNPrs@PEG by UV-VIS spectroscopy.

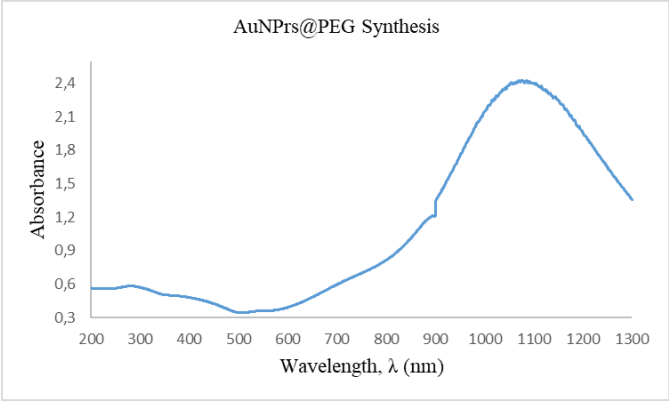

Figure 11 - 3rd quantification of the synthesis for AuNPrs@PEG by UV-VIS spectroscopy.

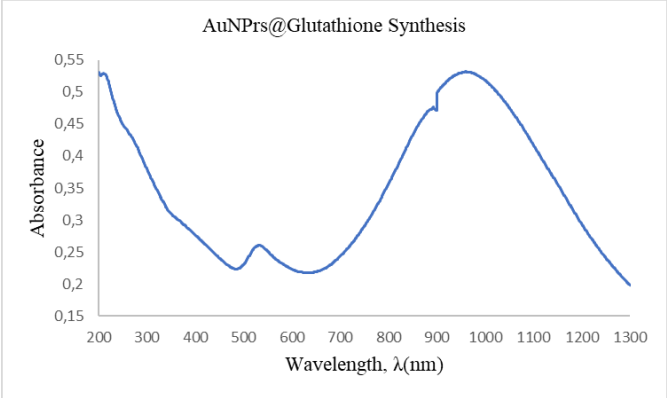

Figure 12 - 1st quantification of the synthesis for AuNPrs@Glutathione by UV-VIS spectroscopy.

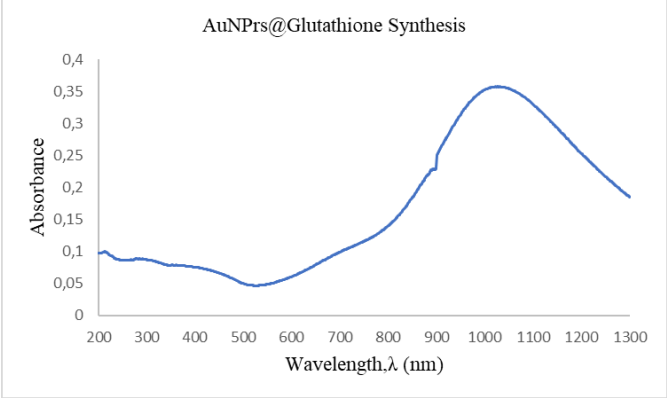

Figure 13 - 2nd quantification of the synthesis for AuNPrs@Glutathione by UV-VIS spectroscopy.

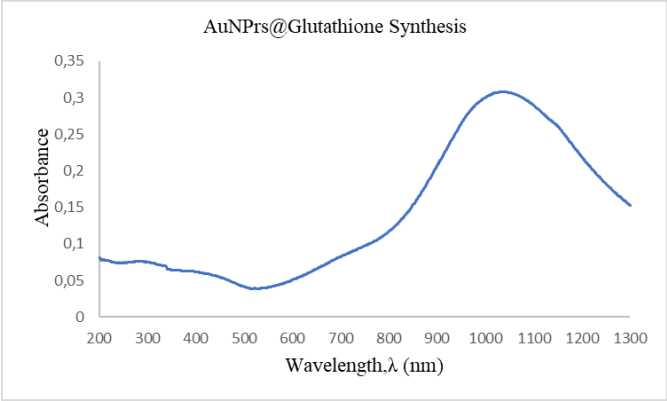

Figure 14 – 3rd quantification of the synthesis for AuNPrs@Glutathione by UV-VIS spectroscopy

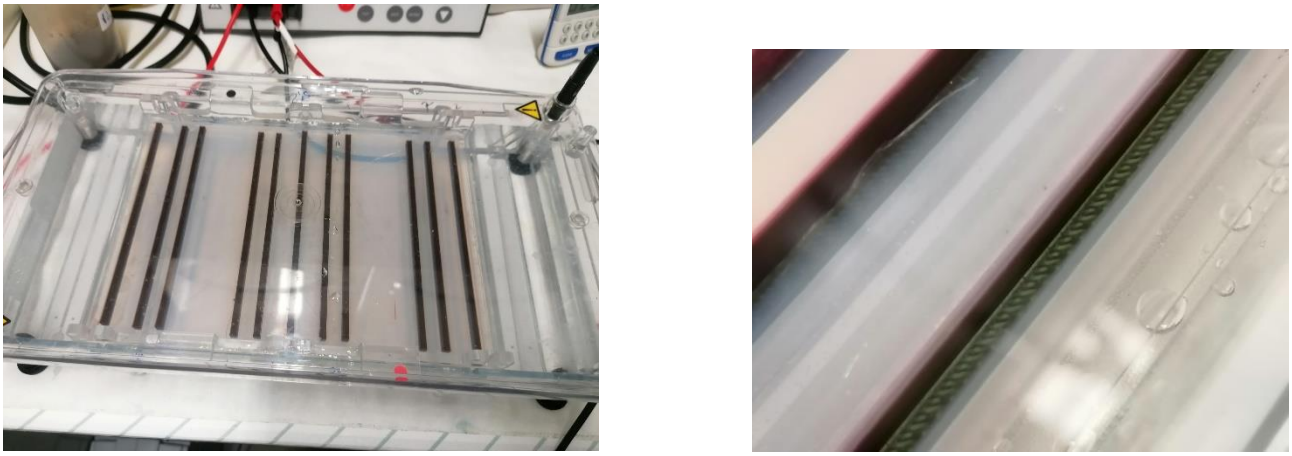

Figure 15 - Image of AuNPrs@PEG during the process of electrophoresis on the left. On the right side of the figure is possible the see the green coloured AuNPrs after electrophoresis.

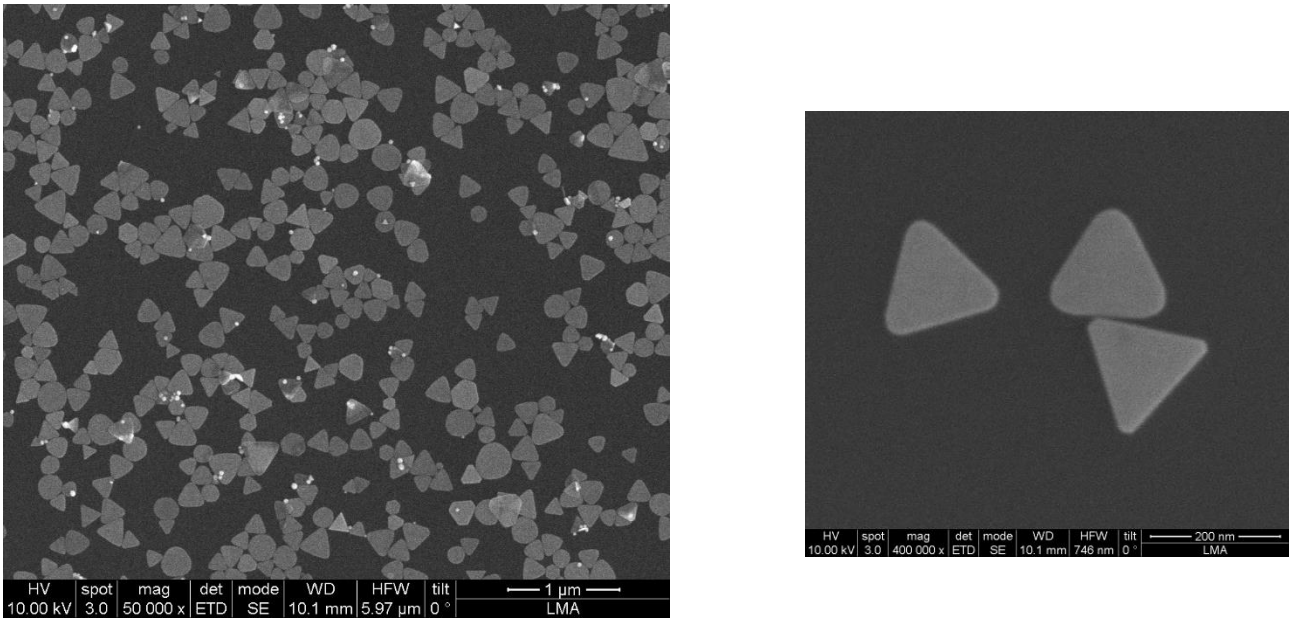

Figure 16 - Images of SEM of the Synthesis for AuNPrs@PEG after purification.

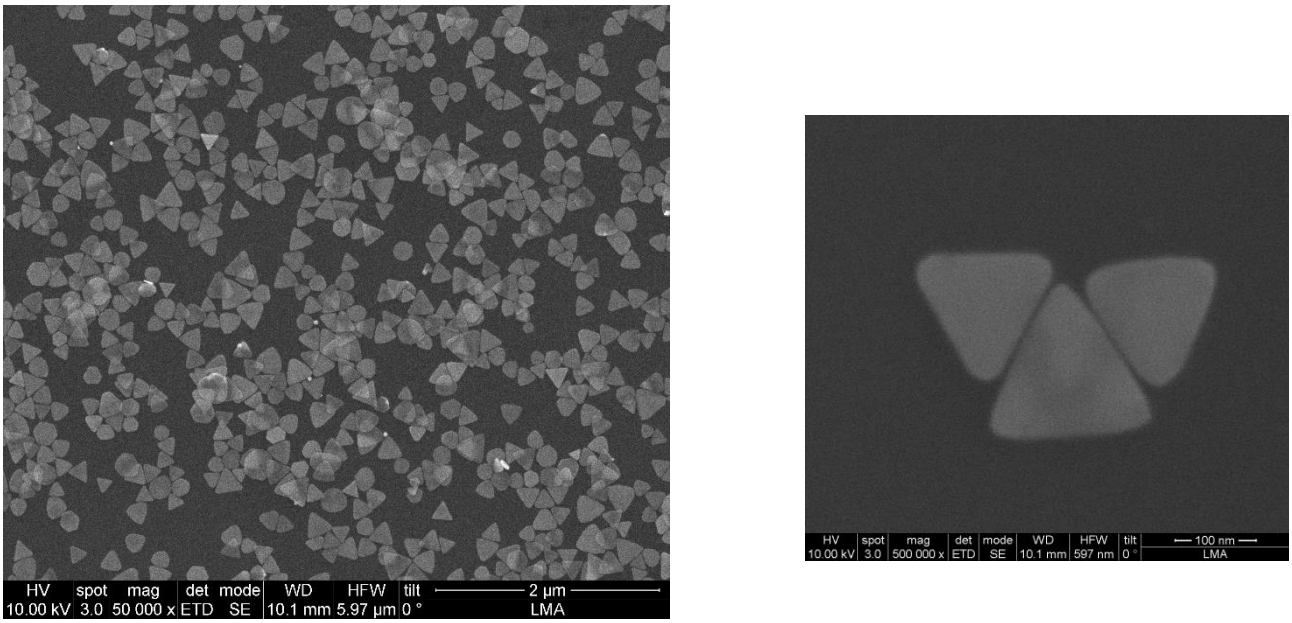

Figure 17 - Images of SEM of the Synthesis for AuNPrs@Glutathione after purification.

A.9 Testing for checking and selecting the best synthesis

Figure 18 - Result of the 0.5pmol sample of Z_2T with AuNPrs@Glutathione after 30 minutes of drying.

Figure 19 - Result of the 0.5pmol sample of of Z_2T with AuNPrs@PEG after 30 minutes of drying.

Figure 20 - Result of the 0.5pmol sample of Z_8T with AuNPrs@Glutathione after 30 minutes of drying.

Figure 21 - Result of the 0.5pmol sample of Z_8T with AuNPrs@PEG after 30 minutes of drying.

A.10 Biofunctionalization of AuNPrs@PEG

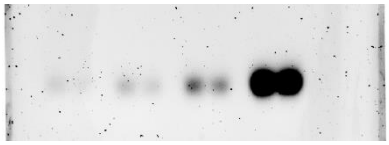

Figure 22 - Gel of biofunctionalization of AuNPrs@PEG with Z_2T. Layout from left to right is Stock and Supernatant, where the concentrations are respectively, [1/16]; [1/8]; [1/4] and [1/1].

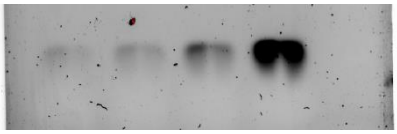

Figure 23 - Gel of biofunctionalization of AuNPrs@PEG with Z_8T. Layout from left to right is Stock and Supernatant, where the concentrations are respectively, [1/16]; [1/8]; [1/4] and [1/1].

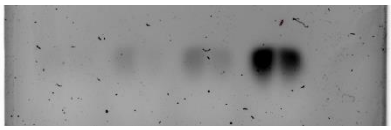

Figure 24 - Gel of biofunctionalization of AuNPrs@PEG with Z_8D. Layout from left to right is Stock and Supernatant, where the concentrations are respectively, [1/16]; [1/8]; [1/4] and [1/1].

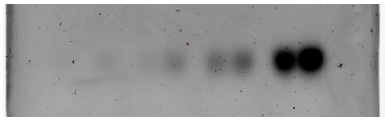

Figure 25 - Gel of biofunctionalization of AuNPrs@PEG with Z_2D. Layout from left to right is Supernatant and Stock, where the concentrations are respectively, [1/16]; [1/8]; [1/4] and [1/1].

A.11 Calibration Curves

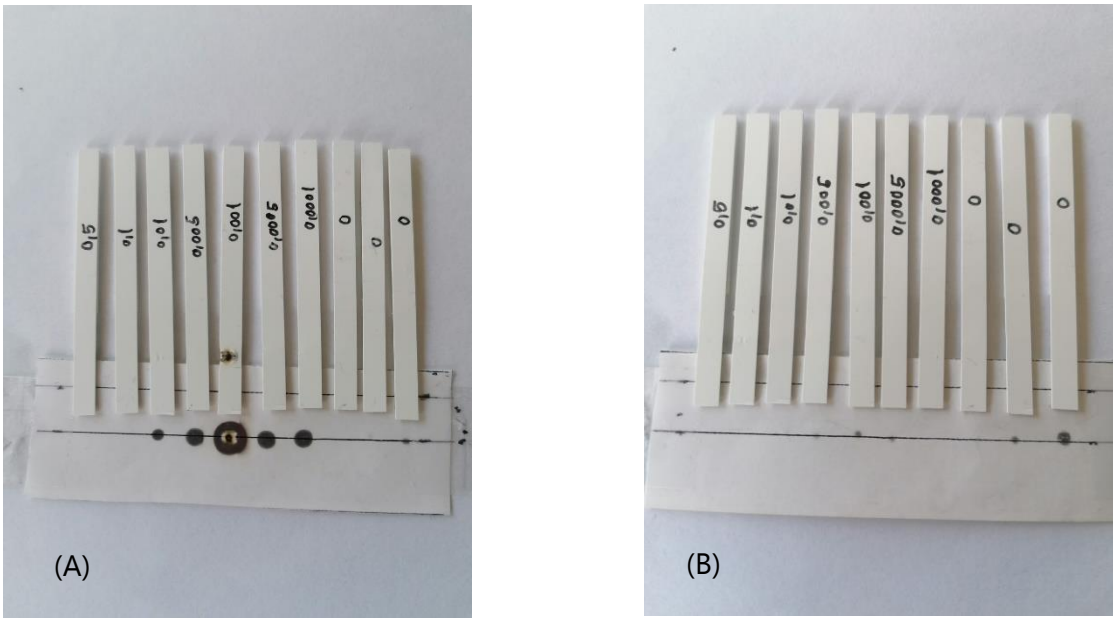

Figure 26 - Example of calibration curves of Z_2T [1/8] irradiated at 72% of power that shows incoherency. Replica (A), the zeros from the left to right were Irradiated at 75%,73% and 72% of power, respectively. Replica (B), all the zeros were Irradiated at 72% of power.

A.12 Optimization of Calibration Curves

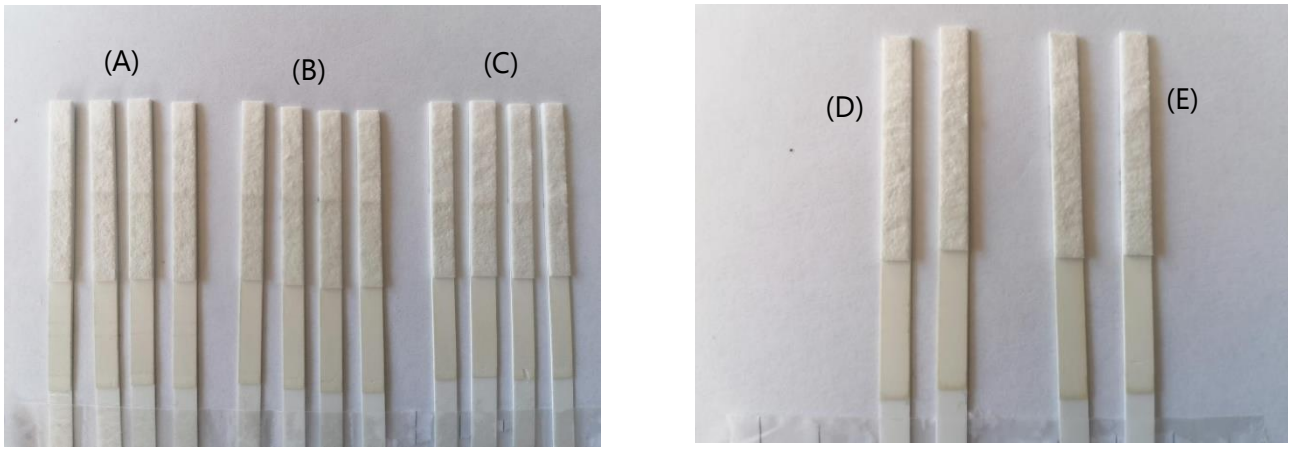

Figure 27 - Optimization for calibration due some variations: (A) Fresh Running Buffer and Tris 50 mM pH 9 100 mM NaCl 50 mM $MgCl_2$; (B) Fresh Running Buffer and MQ water; (C) Old Running Buffer and MQ water; (D) Fresh Running Buffer and Tris 50 mM pH 9 100 mM NaCl 50 mM $MgCl_2$; (E) Fresh Running Buffer and Tris 50 mM pH 9 100 mM NaCl.

A.13 Calibration Curves after Optimization

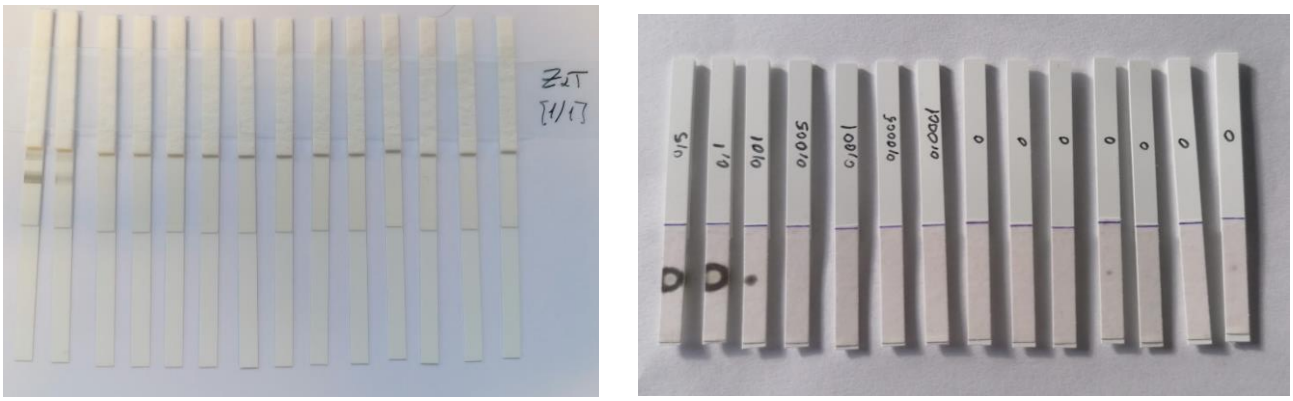

Figure 28 - Calibration Curve for Z_2T [1/1] on the left before irradiation, on the right after irradiated at 68% of NIR laser power.

		Zeros		Samples		
Calibration Curves		Time (seconds)	Irradiation Power (%)	Concentration (pmol)	Time (seconds)	Irradiation Power (%)
Z_2T	[1/1]	60	70	0.5	20	68
			68	0.1	20	
			69	0.01	60	
			69	0.005	60	
			67	0.001	60	
			68	0.0005	60	
			69	0.0001	60	

Table 13 - Time and power of irradiation for positive and negative samples for calibration curve Z_2T for [1/4] concentration.

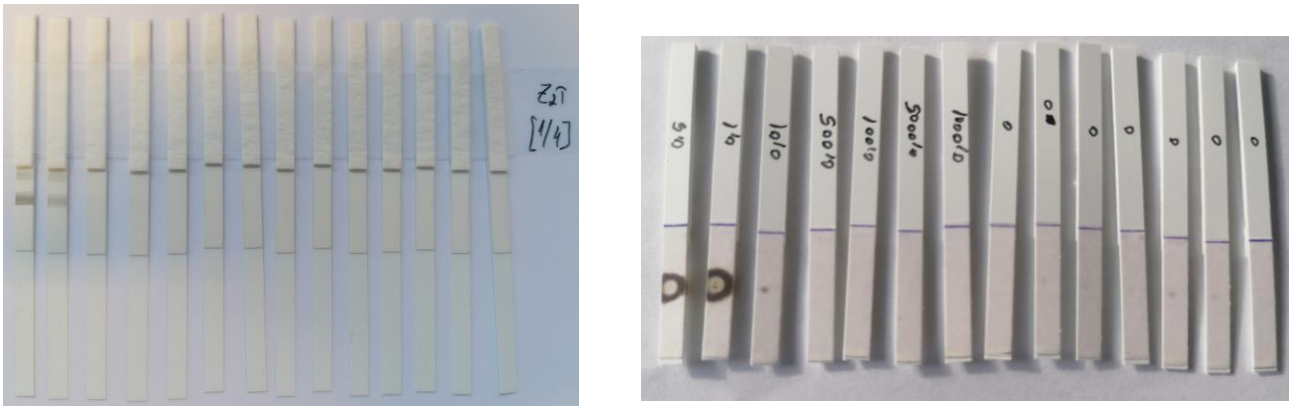

Figure 29 - Calibration Curve for Z_2T [1/4] on the left before irradiation, on the right after irradiated at 68% of NIR laser power.

		Zeros		Samples		
Calibration Curves		Time (seconds)	Irradiation Power (%)	Concentration (pmol)	Time (seconds)	Irradiation Power (%)
Z_2T	[1/4]	60	70	0.5	20	68
			73	0.1	20	
			71	0.01	60	
			69	0.005	60	
			69	0.001	60	
			69	0.0005	60	
			68	0.0001	60	

Table 14 - Time and power of irradiation for positive and negative samples for calibration curve Z_2T for [1/4] concentration.

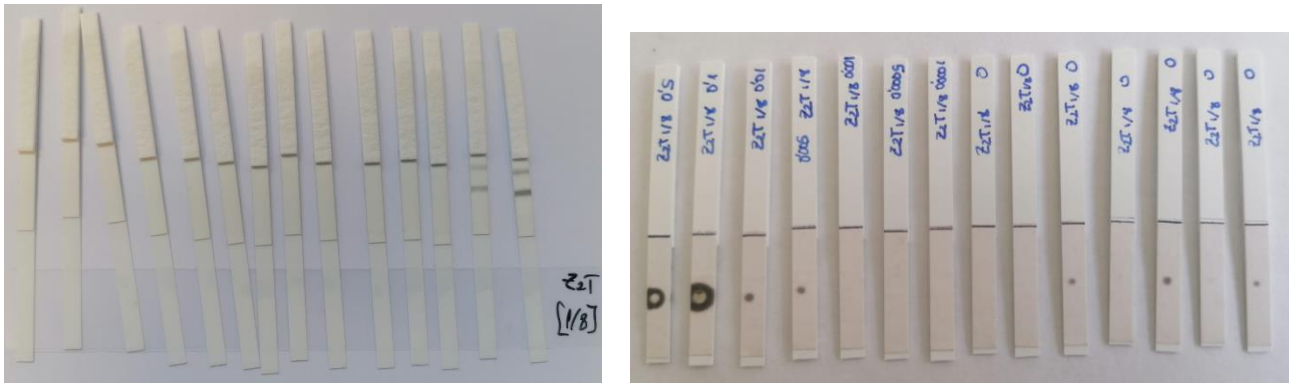

Figure 30 - Calibration Curve for Z_2T [1/8] on the left before irradiation, being the curve start from the left to the right. The figure on the right after irradiated at 62% of NIR laser power.

		Zeros		Samples		
Calibration Curves		Time (seconds)	Irradiation Power (%)	Concentration (pmol)	Time (seconds)	Irradiation Power (%)
Z_2T	[1/8]	60	66	0.5	20	62
			65	0.1	20	
			65	0.01	60	
			65	0.005	60	
			65	0.001	60	
			62	0.0005	60	
			62	0.0001	60	

Table 15 - Time and power of irradiation for positive and negative samples for calibration curve Z_2T for [1/8] concentration.

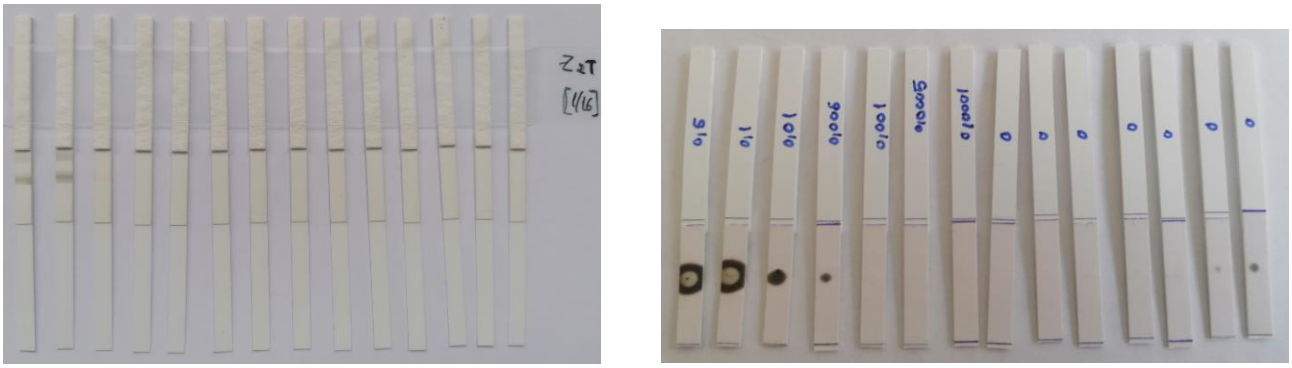

Figure 31 - Calibration Curve for Z_2T [1/16] on the left before irradiation, on the right after irradiated at 64% of NIR laser power.

		Zeros		Samples		
Calibration Curves		Time (seconds)	Irradiation Power (%)	Concentration (pmol)	Time (seconds)	Irradiation Power (%)
Z_2T	[1/16]	60	70	0.5	20	64
			68	0.1	20	
			65	0.01	60	
			64	0.005	60	
			64	0.001	60	
			64	0.0005	60	
			64	0.0001	60	

Table 16 - Time and power of irradiation for positive and negative samples for calibration curve Z_2T [1/16].

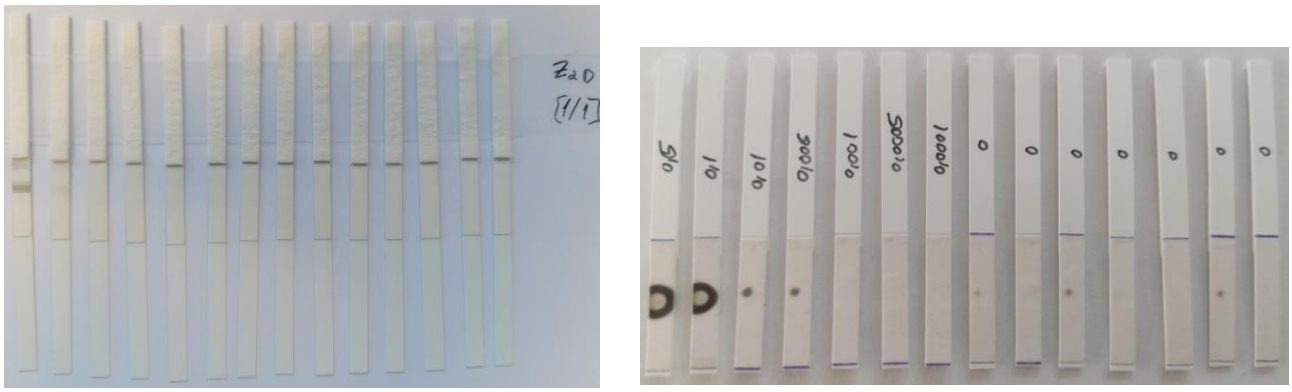

Figure 32 - Calibration Curve for Z_2D [1/1] on the left before irradiation, on the right after irradiated at 67% of NIR laser power.

		Zeros		Samples		
Calibration Curves		Time (seconds)	Irradiation Power (%)	Concentration (pmol)	Time (seconds)	Irradiation Power (%)
Z_2D	[1/1]	60	70	0.5	20	67
			70	0.1	20	
			67	0.01	60	
			67	0.005	60	
			67	0.001	60	
			67	0.0005	60	
			68	0.0001	60	

Table 17 - Time and power of irradiation for positive and negative samples for calibration curve Z_2D [1/1].

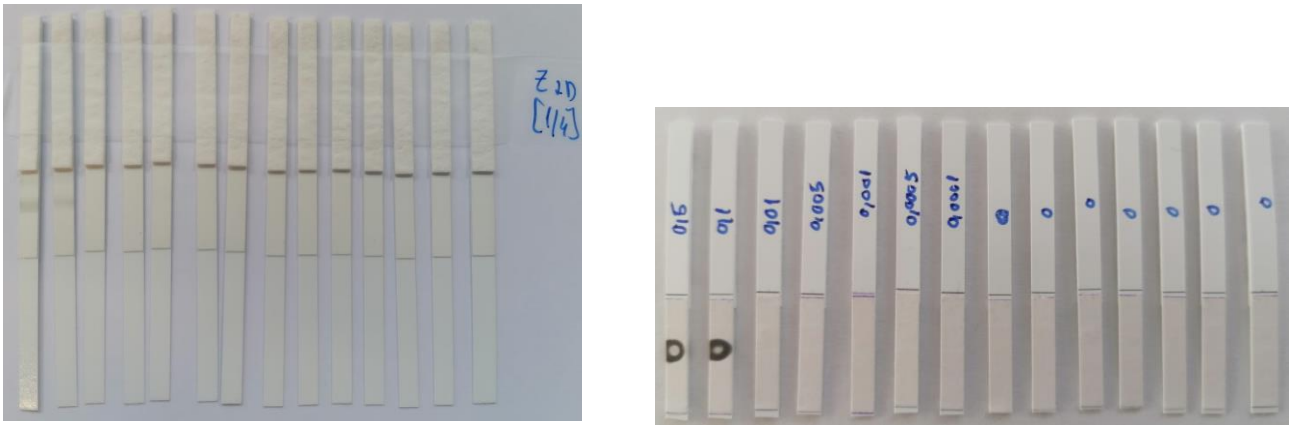

Figure 33 - Calibration Curve for Z_2D [1/4] on the left before irradiation, on the right after irradiated at 68% of NIR laser power.

		Zeros		Samples		
Calibration Curves		Time (seconds)	Irradiation Power (%)	Concentration (pmol)	Time (seconds)	Irradiation Power (%)
Z_2D	[1/4]	60	70	0.5	20	68
			75	0.1	20	
			78	0.01	60	
			70	0.005	60	
			70	0.001	60	
			68	0.0005	60	
			68	0.0001	60	

Table 18 - Time and power of irradiation for positive and negative samples for calibration curve Z_2D [1/4].

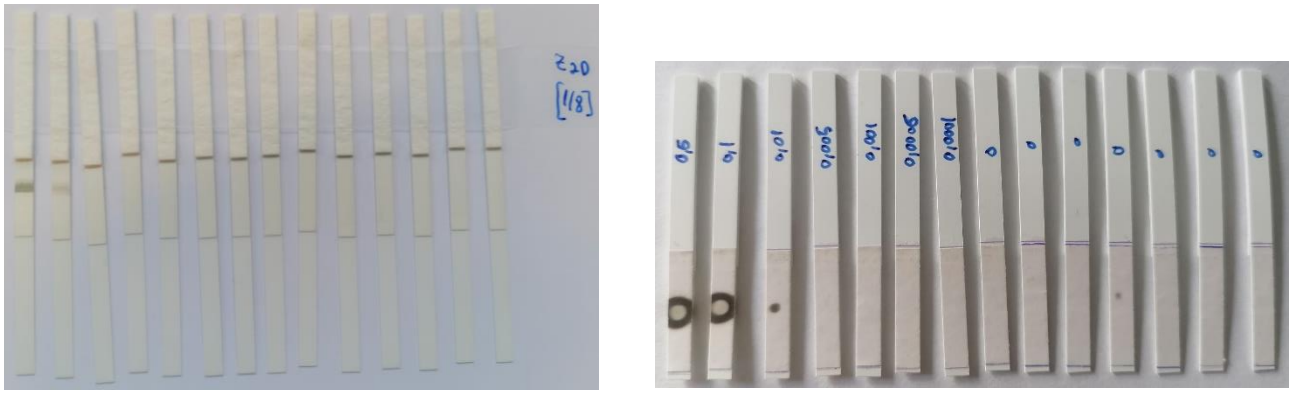

Figure 34 - Calibration Curve for Z_2D [1/8] on the left before irradiation, on the right after irradiated at 65% of NIR laser power.

		Zeros		Samples		
Calibration Curves		Time (seconds)	Irradiation Power (%)	Concentration (pmol)	Time (seconds)	Irradiation Power (%)
Z_2D	[1/8]	60	70	0.5	20	65
			68	0.1	20	
			70	0.01	60	
			75	0.005	60	
			69	0.001	60	
			70	0.0005	60	
			65	0.0001	60	

Table 19 - Time and power of irradiation for positive and negative samples for calibration curve Z_2D [1/8].

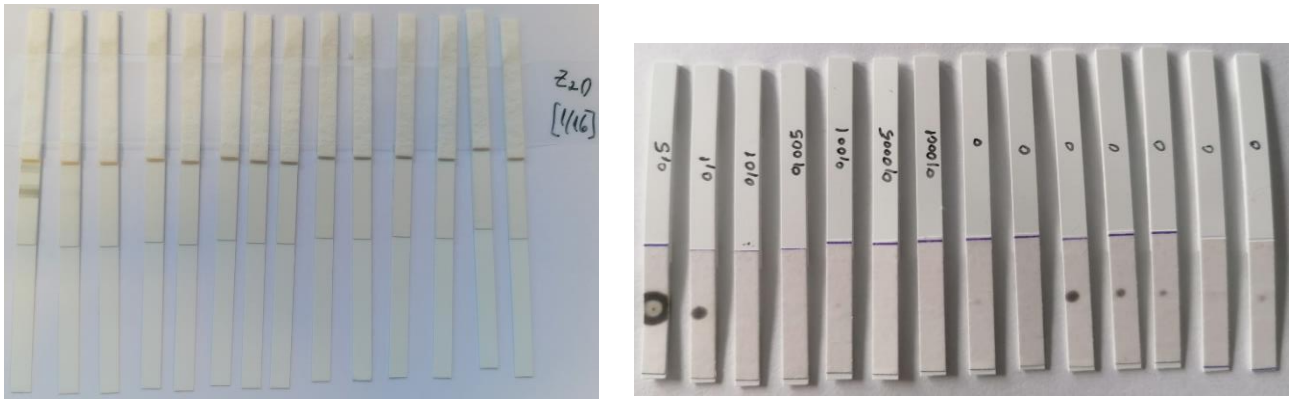

Figure 35 - Calibration Curve for Z_2D [1/16] on the left before irradiation, on the right after irradiated at 65% of NIR laser power.

		Zeros		Samples		
Calibration Curves		Time (seconds)	Irradiation Power (%)	Concentration (pmol)	Time (seconds)	Irradiation Power (%)
Z_2D	[1/8]	60	70	0.5	20	65
			65	0.1	60	
			72	0.01	60	
			69	0.005	60	
			67	0.001	60	
			65	0.0005	60	
			67	0.0001	60	

Table 20 - Time and power of irradiation for positive and negative samples for calibration curve Z_2D [1/16].

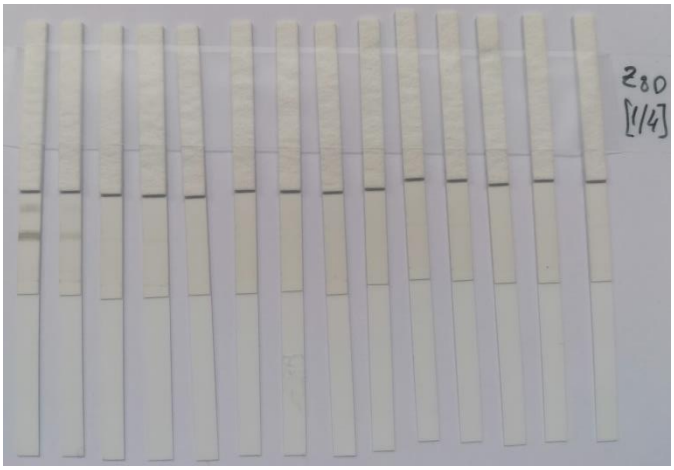

Figure 36 – Example of Calibration Curve with aggregation before irradiation for Z_8D [1/4].

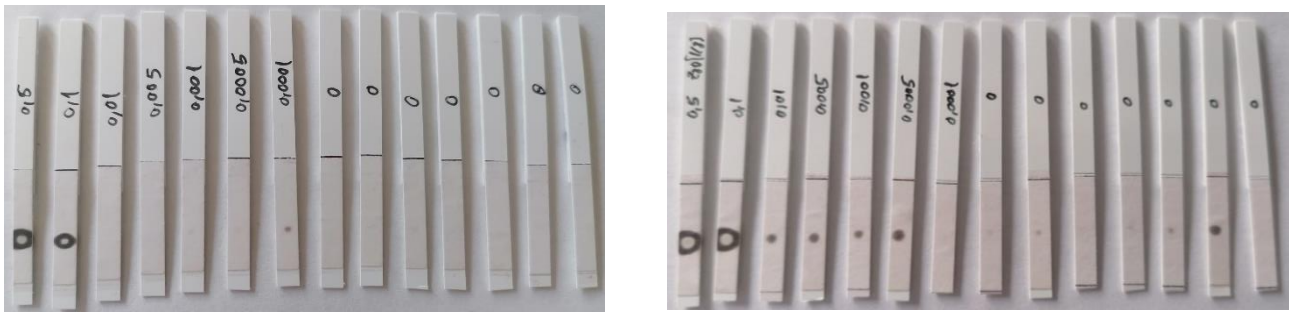

Figure 37 - Examples of calibration curves irradiated with aggregation. On the left Z_8T [1/4] and on the right Z_8D [1/8], both irradiated at 65% of NIR laser power.

Zeros			Samples		
Time (seconds)	Irradiation Power (%)		Concentration (pmol)	Time (seconds)	Irradiation Power (%)
	Z_8T [1/4]	Z_8D [1/8]			
60	60	70	0.5	10	65
	65	70	0.1	10	
	63	65	0.01	60	
	65	65	0.005	60	
	65	60	0.001	60	
	65	60	0.0005	60	
	65	65	0.0001	60	

Table 21 - Time and power of irradiation for positive and negative samples for calibrations curves with aggregation, namely Z_8T [1/4] and Z_8D [1/8].

A.14 Calibration Curves for Viral Transport Media

Figure 38 - Viral Transport Way: DeltaLab on the left and Biocomma on the right.

Figure 39 - Example of Z_2T [1/16] in DeltaLab matrix, with Tris 50 mM pH 9 100 mM NaCl showing the presence of ghost effect.

A.15 Optimization for Viral Transport Media

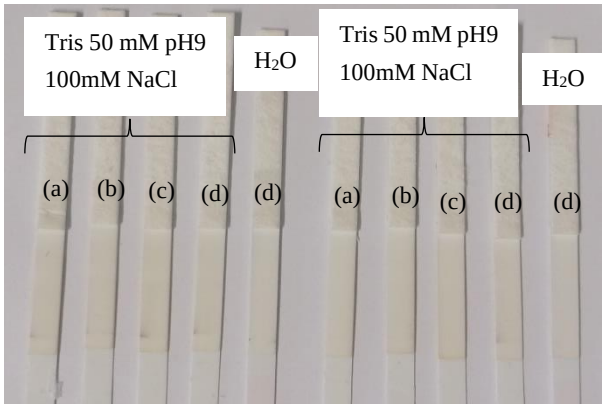

Figure 40 - Testing negative samples of Z_2T [1/16] and Z_2D [1/16] in DeltaLab matrix with Tris 50 mM pH 9 100mM NaCl and MQ water for different RBs: (a) PBS 1x pH 7.4 BSA 0.5% T_{20} 1%; (b) Buffer Phosphate 10 mM pH 7.4; (c) Hepes 10 mM pH 7.4 and (d) PBS 10x pH 7.4 BSA 0.5% T_{20} 1%. Where the firsts five ones are Z_2T [1/16] and the last five are Z_2D [1/16].

Figure 41 - Testing 0,5pmol target in DeltaLab matrix using pre-incubation of 15 minutes (right) and without pre-incubation (left).

A.16 Calibration Curves for Viral Transport media after optimization

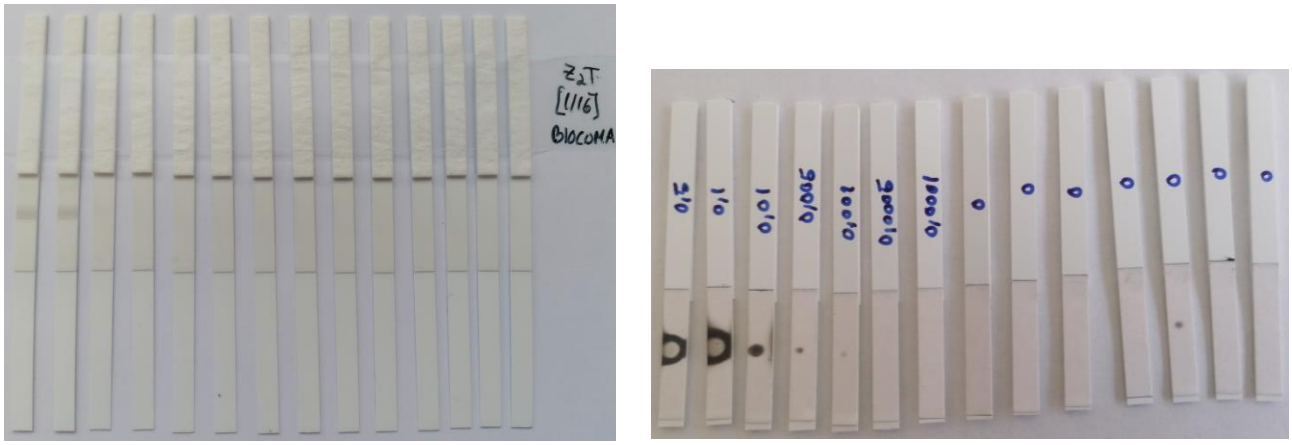

Figure 42 - Calibration Curve for Z_2T [1/16] Biocoma matrix: on the left before irradiation, on the right after irradiated at 72% of NIR laser power.

		Zeros		Samples		
Calibration Curves		Time (seconds)	Irradiation Power (%)	Concentration (pmol)	Time (seconds)	Irradiation Power (%)
Z_2T	[1/16]	60	70	0.5	20	72
			75	0.1	20	
			75	0.01	60	
			70	0.005	60	
			72	0.001	60	
			70	0.0005	60	
		50	72	0.0001	60	

Table 22 - Time and power of irradiation for positive and negative samples for calibration curve Z_2T [1/16] in Biocomma matrix.

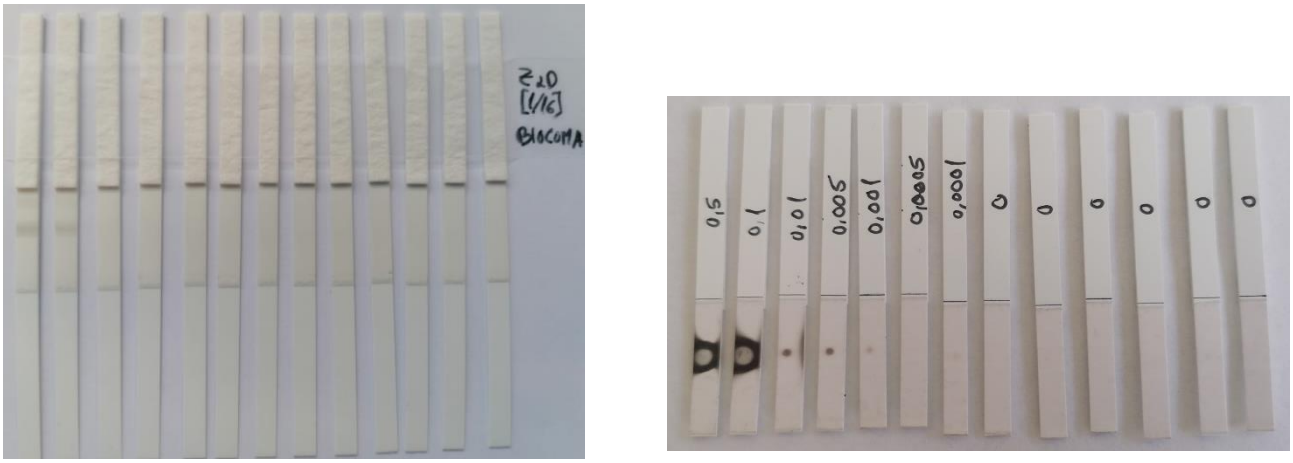

Figure 43 - Calibration Curve for Z_2D [1/16] in Biocoma matrix: on the left before irradiation, on the right after irradiated at 74% of NIR laser power.

		Zeros		Samples		
Calibration Curves		Time (seconds)	Irradiation Power (%)	Concentration (pmol)	Time (seconds)	Irradiation Power (%)
Z_2D	[1/16]	60	70	0.5	20	74
			75	0.1	20	
			73	0.01	60	
			74	0.005	60	
			74	0.001	60	
			73	0.0005	60	
		-	-	0.0001	60	

Table 23 - Time and power of irradiation for positive and negative samples for calibration curve Z_2D [1/16] in Biocomma matrix

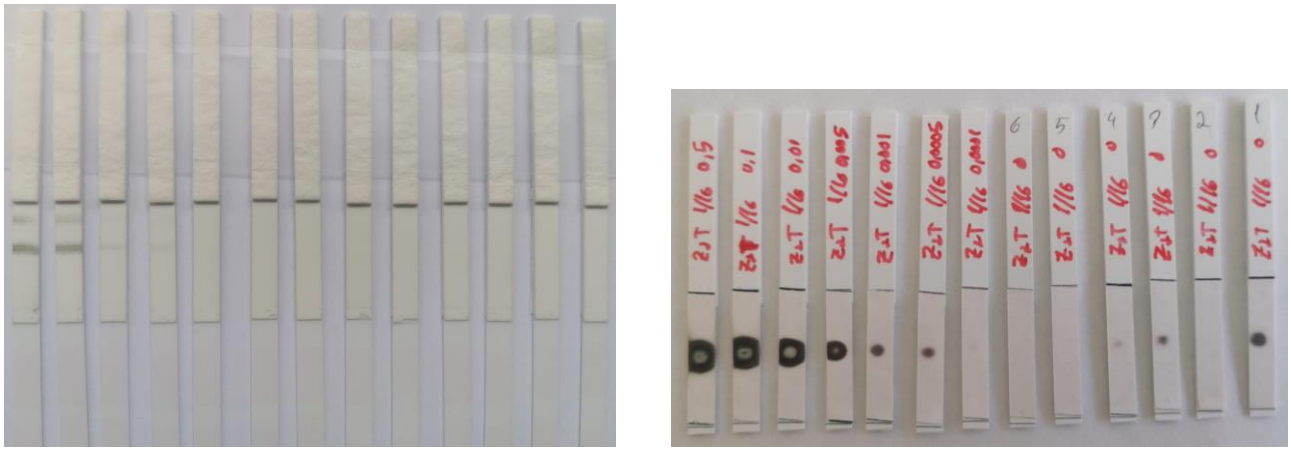

Figure 44 - Calibration Curve for Z_2T [1/16] in DeltaLab matrix: on the left before irradiation, on the right after irradiated at 78% of NIR laser power.

		Zeros		Samples		
Calibration Curves		Time (seconds)	Irradiation Power (%)	Concentration (pmol)	Time (seconds)	Irradiation Power (%)
Z_2T	[1/16]	60	85	0.5	10	78
			80	0.1	10	
			83	0.01	10	
			80	0.005	10	
			78	0.001	60	
			78	0.0005	60	
		-	-	0.0001	60	

Table 24 - Time and power of irradiation for positive and negative samples for calibration curve Z_2T [1/16] in DeltaLab matrix.

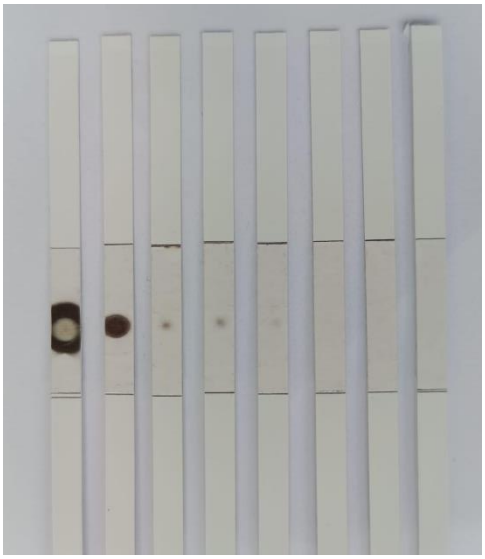

Figure 45 - Calibration Curve for Z_2D [1/16] in DeltaLab matrix irradiated at 63% of NIR laser power, except last samples that is a blank.

		Zeros		Samples		
Calibration Curves		Time (seconds)	Irradiation Power (%)	Concentration (pmol)	Time (seconds)	Irradiation Power (%)
Z_2D	[1/16]	30	78	0.5	10	63
		50	70	0.1	10	
		60	65	0.01	60	
		60	63	0.005	60	
		60	63	0.001	60	
		60	63	0.0005	60	
		-	-	0.0001	60	

Table 25 - Time and power of irradiation for positive and negative samples for calibration curve Z_2D [1/16] in DeltaLab matrix.

A.17 Real Samples

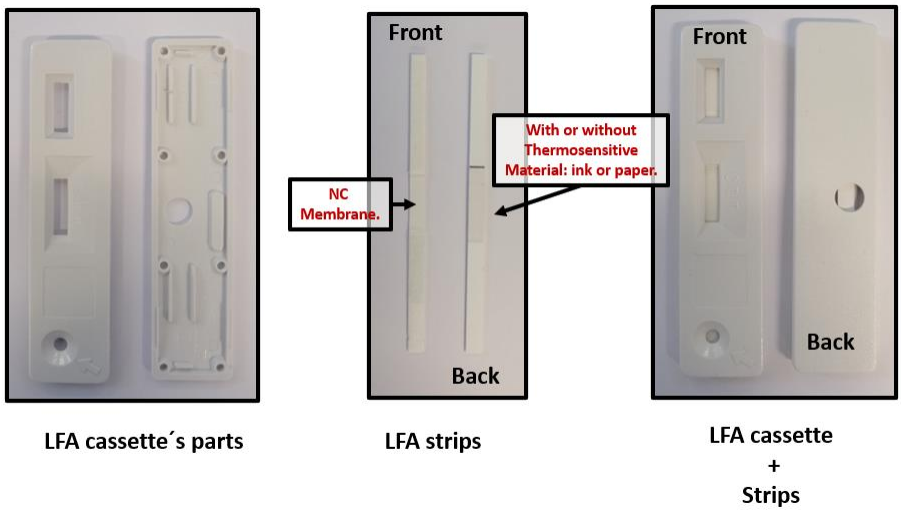

Figure 46 - Example of how the stripes are prepared for deposition of the samples and NIR laser irradiation.

Figure 47 – Test of real samples for Z_2T [1/16] in DeltaLab matrix irradiated at 61% of NIR laser power.

	Zeros			Samples			
	Negative samples reference	Time (seconds)	Irradia-tion Power (%)	Type	Positive samples reference	Time (seconds)	Irradiation Power (%)
Real Samples using Z_2T [1/16]	5956	50	65	A	1887	75	61
		60	60		9725		
		90	59		1671		
		90	60		6586		
	6885	50	63		8658		
		90	61	B	0576		
		75	61				
		75	61				

Table 26 - Time and power of irradiation for positive and negative samples for real samples using Z_2T [1/16] in DeltaLab ® matrix.

A.18 Specificity Tests

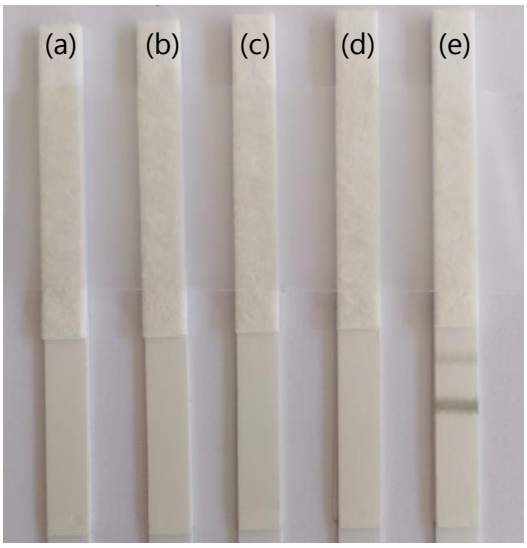

Figure 48 - Test of specificity for Z_2T [1/16] for different target solution of 0.5pmol mixed with DeltaLab matrix: (a) RSV1; (b) RSV2; (c) cc1; (d) Z_8 and (e) Z_2.

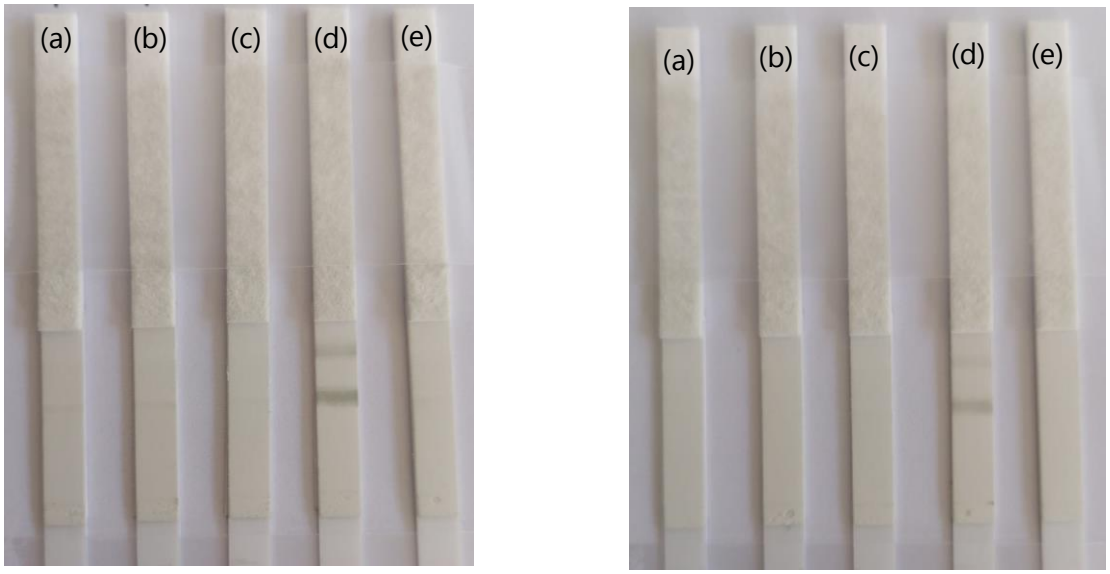

Figure 49 - Test of specificity for Z_8T [1/1] (left) and Z_8D [1/1] (right) for different target solution of 0.5 pmol mixed with DeltaLab matrix: (a) RSV1; (b) RSV2; (c) cc1; (d) Z_8 and (e) Z_2.